# A Method for Retrieving Coarse-Resolution Leaf Area Index for Mixed Biomes Using a Mixed-Pixel Correction Factor

Yadong Dong[ID], Jing Li, Ziti Jiao[ID], Qinhuo Liu[ID], *Senior Member, IEEE*, Jing Zhao[ID], Baodong Xu[ID], Hu Zhang[ID], Zhaoxing Zhang, Chang Liu, Yuri Knyazikhin[ID], and Ranga B. Myneni

*Abstract*—The leaf area index (LAI) is a key structural parameter of vegetation canopies. Accordingly, several moderate-resolution global LAI products have been produced and widely used in the field of remote sensing. However, the accuracy of the current moderate-resolution global LAI products cannot satisfy the requirements recommended by the LAI application communities, especially in heterogeneous areas composed of mixed land cover types. In this study, we propose a mixed-pixel correction (MPC) method to improve the accuracy of LAI retrievals over heterogeneous areas by considering the influence of heterogeneity caused by the mixture of different biome types with the help of high-resolution land cover maps. The DART-simulated LAI, the aggregated Landsat LAI, and the site-based high-resolution LAI reference maps are used to evaluate the performance of the MPC method. The results indicate that the MPC method can reduce the influences of spatial heterogeneity and biome misclassification to obtain the LAI with much better accuracy than the Moderate Resolution Imaging Spectroradiometer (MODIS) main algorithm, given that the high-resolution land cover map is accurate. The root mean square error (RMSE) (bias) decreases from 0.749 (0.486) to 0.414 (0.087), while the R2 increases from 0.084 to 0.524, and the proportion of pixels that fulfill the uncertainty requirement of the GCOS increases from 38.2% to 84.6% for the results of site-based high-resolution LAI reference maps. Spatially explicit information about vegetation fractional cover can further reduce uncertainties induced by variations in canopy density for the results of DART simulated data. The proposed method shows potential for improving global moderate-resolution LAI products.

*Index Terms*—Biome misclassification, land cover mixture, leaf area index (LAI), Moderate Resolution Imaging Spectroradiometer (MODIS).

Yadong Dong, Jing Zhao, and Zhaoxing Zhang are with the State Key Laboratory of Remote Sensing Science, Jointly Sponsored by the Aerospace Information Research Institute, Chinese Academy of Sciences and Beijing Normal University, Beijing 100101, China (e-mail: dongyd@aircas.ac.cn; zhaojing1@radi.ac.cn; zhangzhaoxing@aircas.ac.cn).

Jing Li, Qinhuo Liu, and Chang Liu are with the State Key Laboratory of Remote Sensing Science, Jointly Sponsored by the Aerospace Information Research Institute, Chinese Academy of Sciences and Beijing Normal University, Beijing 100101, China, and also with the College of Resources and Environment, University of Chinese Academy of Sciences, Beijing 100049, China (e-mail: lijing200531@aircas.ac.cn; liuqh@radi.ac.cn; liuchang193@mails.ucas.ac.cn).

Ziti Jiao is with the State Key Laboratory of Remote Sensing Science, Jointly Sponsored by the Aerospace Information Research Institute, Chinese Academy of Sciences and Beijing Normal University, Beijing 100101, China, and also with the Beijing Engineering Research Center for Global Land Remote Sensing Products, Institute of Remote Sensing Science and Engineering, Faculty of Geographical Science, Beijing Normal University, Beijing 100875, China (e-mail: jiaozt@bnu.edu.cn).

Baodong Xu is with the Macro Agriculture Research Institute, College of Resource and Environment, Huazhong Agricultural University, Wuhan 430070, China (e-mail: xubaodong@mail.hzau.edu.cn).

Hu Zhang is with the College of Urban and Environmental Sciences, Tianjin Normal University, Tianjin 300387, China (e-mail: askzhanghu@126.com).

Yuri Knyazikhin and Ranga B. Myneni are with the Department of Earth and Environment, Boston University, Boston, MA 02215 USA (e-mail: jknjazi@bu.edu; ranga.myneni@gmail.com).

Digital Object Identifier 10.1109/TGRS.2023.3235949

## I. INTRODUCTION

THE leaf area index (LAI), which is defined as one-half of the total green leaf area per unit horizontal ground surface area [1], is a key structural parameter of the vegetation canopy [2], [3]. Accordingly, the LAI is listed as an essential climate variable (ECV) by the Global Climate Observing System (GCOS) [4] and in the monitoring of progress toward the Aichi Biodiversity Targets [5]. It has been widely used in the study of global climate change [6], the estimation of fractional vegetation cover (FVC) [7] and global primary productivity (GPP) [8], the monitoring of vegetation growth [9], and the modeling of mass, energy, and momentum exchanges between the biosphere and the atmosphere [10], [11], [12], [13], [14], [15].

Several global LAI products have been produced from the surface reflectance data observed by moderate-resolution sensors, such as the Moderate Resolution Imaging Spectroradiometer (MODIS) [16], [17], [18], the Advanced Very High Resolution Radiometer (AVHRR) [18], [19], the Visible Infrared Imaging Radiometer Suite (VIIRS) [20], the VEGETATION [21], [22], PROBA-V, [23], [24], and the Medium-Resolution Imaging Spectrometer (MERIS) [25]. These products have been extensively validated in various studies based on field measurements and upscaled high-resolution LAI reference maps [26], [27], [28], [29], [30], [31], [32], [33], [34], [35], [36], [37], [38], [39]. The root mean square error (RMSE) between major moderate-resolution LAI products and the reference data ranged from 0.19 to 2.41,

and its median value was 0.88 [40]. However, the accuracy of the current moderate-resolution global LAI products does not satisfy the requirements recommended by LAI application communities, such as the GCOS [<max(0.5, 20%)] [4], especially in heterogeneous areas composed of different land cover types [41].

Uncertainties in the retrieval algorithm and input land cover maps are two key factors that influence the accuracy of LAI retrievals [42]. In heterogeneous areas composed of different land cover types, the application of retrieval algorithms proposed for homogeneous surfaces introduces a strong scale effect in LAI estimation since the assumption of homogeneous surfaces is no longer valid [43]. In addition, the mixture of different land cover types increases the possibility of biome misclassification for coarse-resolution pixels. Therefore, the influence of mixed land cover types and biome misclassification should be analyzed and corrected to obtain a more accurate LAI.

Several studies have shown that mixed land cover types and biome misclassification generally lead to large errors in the generation of moderate-resolution LAI products [41], [44], [45], [46], [47]. The relative scaling effects of the LAI caused by spatial heterogeneity may be up to 50% for mixed pixels [48]. Tian et al. [44] found that the LAI retrieval errors of heterogeneous pixels were negatively correlated with the proportions of the dominant biome types, and large LAI retrieval errors could be found for nonforest-dominated pixels mixed with forests, and vice versa. Fang et al. [47] analyzed the LAI uncertainties induced by biome misclassification and concluded that the misclassification of savannas as broadleaf crops led to a considerably overestimated LAI with the largest bias of 0.84 m$^2$/m$^2$ (100.0%). In addition, mixtures of different vegetation types are ubiquitous at low- and moderate-resolution scales. According to statistics based on the 30-m Global Land Cover Dataset (GlobalLand30) of the global land area [49], the proportion of pixels with a mixture of different land cover types can exceed 65% at the 1-km scale [50]. Therefore, the accuracy of the retrieved LAI will be greatly improved if the effects of mixed land cover types and biome misclassification are considered and corrected for the retrieval of global moderate-resolution LAI products [43], [51].

The high-resolution LAI products derived based on higher resolution reflectance data (e.g., Landsat and SPOT) and/or field measurements can reduce scale differences caused by spatial heterogeneity. Thus, upscaled high-resolution LAI reference maps are widely used in the validation of coarse-resolution LAI products [40]. Reduce the effects of spatial heterogeneity by upscaling the high-resolution LAI products to the desired moderate-resolution scale when high-resolution reflectance data are available in the calculation of moderate-resolution LAI and may be a simple solution. However, due to the long revisit frequency (e.g., 16 days for the Landsat-8 sensor), in most cases, matched high-resolution reflectance data cannot be found in the calculation of the moderate-resolution LAI product because the input moderate-resolution data have a much shorter revisit

frequency (e.g., every one to two days for the MODIS sensor).

Several efforts have been made to reduce the effect of mixed land cover types on the retrieval of LAI products. Jin et al. [46] developed a spatial scaling algorithm to improve the accuracy of LAI retrievals at the 960-m scale based on an empirical linear relationship between the correction factor and the proportion of the dominant biome type. However, only three land cover types (i.e., conifers, mixed forests, and open lands) were used in the algorithm, and an empirical method may not be applicable on a global scale. Wu et al. [43] developed a joint algorithm to reduce the effect of heterogeneity caused by both density variation in vegetation cover and a mixture of different biome types. The algorithm was improved by Yin et al. [51] to further consider the mixture of vegetation and nonvegetation. These algorithms were validated using a simulated image constructed from a classification map [43] and a Landsat5/TM image that covered the study area in the middle reach of the Heihe River Basin in Northwest China [51]. The results indicated that the proposed algorithms greatly reduced the retrieval errors caused by the scaling effects. However, the LAI retrieval method used in the evaluation of the proposed algorithms was a simple transfer relationship between the normalized difference vegetation index (NDVI) and LAI. These algorithms may not be appropriate for the retrieval model with strong nonlinearity (e.g., the main algorithm of the MODIS LAI product) since they neglect the third-order and higher Taylor expansion terms [43]. Zeng et al. [52] proposed the Radiative Transfer Model for Patchy Ecotones (RTEC), which can accurately simulate the directional reflectance of mixed pixels over heterogeneous areas and, thus, can be used to retrieve LAI products with improved accuracy over heterogeneous areas. However, because the RTEC model is computationally time-consuming, it is difficult to apply this model to retrieve moderate-resolution LAI products at the global scale [52]. Xu et al. [41] corrected the effect of land–water mixtures by considering the negative deviation of the reflectance induced by water. This method can significantly improve the accuracy of LAI retrievals from land–water mixed pixels and has the potential to improve the quality of global LAI products. Through the use of a high-resolution land cover map to reduce the errors of land–water mixed pixels, Xu et al. [41] provided a new idea to reduce the errors of land cover mixtures for LAI retrievals. However, to date, no available method has been developed that can reduce the effects of mixed land cover types with different vegetation biome types and biome misclassification on the retrieval of global moderate-resolution LAI products.

In this study, we propose a mixed-pixel correction (MPC) method to improve the accuracy of LAI retrievals over heterogeneous areas composed of a mixture of different vegetation biome types based on an MPC factor (MPCF). In the method, the influence of heterogeneity caused by the mixture of different biome types is considered, with the help of high-resolution land cover maps. The MPC method is used to correct the LAI retrieved by the main algorithm of the MODIS LAI product [16] to evaluate its performance. Scenes simulated by

the discrete anisotropic radiative transfer (DART) model, the aggregated 30-m Landsat LAI, and site-based high-resolution LAI reference maps are used to assess the accuracy of the proposed MPC method.

## II. Framework of the MPC Method

For a mixed pixel composed of $n$ subpixels, the application of LAI retrieval algorithms proposed for homogeneous surfaces introduces large uncertainties because the single biome type used in the operational algorithms of moderate-resolution LAI products cannot effectively capture the vegetation biochemical and structural characteristics of the mixed pixel (e.g., clumping effect and leaf angular distribution). In this article, we propose a correction factor, referred to as MPCF, to capture such derivation caused by the mixture of different biome types. The MPCF of a mixed pixel is defined as the ratio of the mixed-pixel LAI estimated based on the LAI retrieval models proposed for a certain homogeneous biome type a ($L_{\text{model\_a}}$) to the real LAI of the mixed pixel ($L_m$) calculated by the arithmetic average of the subpixel LAI

$$\text{MPCF} = \frac{L_{\text{model\_a}}}{L_m} = \frac{L_{\text{model\_a}}}{\frac{1}{n}\sum_{i=1}^{n} L_i} \tag{1}$$

where $L_i$ is the LAI of subpixel $i$. $L_m$ represents the real LAI of the mixed pixel, which is the arithmetic average of subpixel LAI, and $n$ is the number of subpixels. $L_{\text{model\_a}}$ is the model-inversed LAI when the mixed-pixel reflectance is treated as the reflectance of the canopy covered by biome type a. It is a usual way to estimate the mixed-pixel LAI by treating the mixed pixel reflectance as the reflectance of the canopy covered by the biome type a in the algorithms of present LAI products. MPCF represents the mixing effect of the biome-type mixture in this pure-vegetation-assumption inversion. If the pixel is pure and homogenous, then MPCF = 1. If the pixel is mixed with forests and herbaceous plants, and its LAI is inversed using the biome type of forests, then MPCF > 1 since the inversed forest LAI is usually greater than the inversed herbaceous LAI when the input reflectance and angular information are the same. In contrast, if the LAI of forest-herbaceous mixed pixels is inversed using the biome type of herbaceous, then MPCF < 1. Based on the definition of MPCF, the LAI inversion of a mixed pixel can be translated into the inversion of a specific pure vegetation type (e.g., biome type a).

$L_i$ can be expressed as follows according to the modified Beer's law [53]:

$$L_i = -\frac{\cos\theta \ln P_i(\theta)}{G_i(\theta)\Omega_i} \tag{2}$$

where $\theta$ is the view zenith angle. $P_i(\theta)$ and $\Omega_i$ are the gap proportion and the clumping index (CI) of subpixel $i$, respectively. $G_i(\theta)$ is the foliage projection coefficient that characterizes the foliage angular distribution of subpixel $i$. Then, (1) becomes

$$\text{MPCF} = \frac{L_{\text{model\_a}}}{\frac{1}{n}\sum_{i=1}^{n} L_i} = \frac{-\frac{\cos\theta \ln P_{\text{model\_a}}(\theta)}{G_{\text{model\_a}}(\theta)\Omega_{\text{model\_a}}}}{-\frac{1}{n}\sum_{i=1}^{n}\frac{\cos\theta \ln P_i(\theta)}{G_i(\theta)\Omega_i}}$$

$$= \frac{\ln P_{\text{model\_a}}(\theta)}{\frac{1}{n}\sum_{i=1}^{n}\frac{\ln P_i(\theta)}{\frac{G_i(\theta)}{G_{\text{model\_a}}(\theta)}\cdot\frac{\Omega_i}{\Omega_{\text{model\_a}}}}} \tag{3}$$

where $\Omega_{\text{model\_a}}$, $G_{\text{model\_a}}(\theta)$, and $P_{\text{model\_a}}(\theta)$ are the CI, the foliage projection coefficient, and the gap proportion estimated with the moderate-resolution mixed-pixel reflectance by an LAI retrieval model under the assumption that the whole pixel is covered by biome type a. From (3), the MPCF is related to the clumping effect, leaf angular distribution and gap proportion of the subpixels.

Generally, the CI values of the same biome type are usually assumed to be invariant in the application of CI to the LAI retrieval algorithm [54]. Based on this, we assume that the CI value of biome type bio_$i$ (bio_$i$ is the corresponding biome type of subpixel $i$) used in an LAI retrieval model ($\Omega_{\text{model\_bio\_}i}$) can well capture the clumping effect of subpixels of biome type bio_$i$, meaning that $\Omega_{\text{model\_bio\_}i}$ is the same as the CI values of subpixels of biome type bio_$i$ (i.e., $\Omega_{\text{model\_bio\_}i} = \Omega_i$). Then, $\Omega_i/\Omega_{\text{model\_a}}$ can be expressed as follows according to the modified Beer's law [53]:

$$\frac{\Omega_i}{\Omega_{\text{model\_a}}} = \frac{\Omega_{\text{model\_bio\_}i}}{\Omega_{\text{model\_a}}} = \frac{-\frac{\cos\theta \ln P_{\text{model\_bio\_}i}(\theta)}{G_{\text{model\_bio\_}i}(\theta)L_{\text{model\_bio\_}i}}}{-\frac{\cos\theta \ln P_{\text{model\_a}}(\theta)}{G_{\text{model\_a}}(\theta)L_{\text{model\_a}}}}$$

$$= \frac{G_{\text{model\_a}}(\theta)}{G_{\text{model\_bio\_}i}(\theta)}\frac{L_{\text{model\_a}}}{L_{\text{model\_bio\_}i}}\frac{\ln P_{\text{model\_bio\_}i}(\theta)}{\ln P_{\text{model\_a}}(\theta)} \tag{4}$$

where $\Omega_{\text{model\_bio\_}i}$, $G_{\text{model\_bio\_}i}(\theta)$, $P_{\text{model\_bio\_}i}(\theta)$, and $L_{\text{model\_bio\_}i}$ are the CI, the foliage projection coefficient, gap proportion, and LAI, respectively, estimated with the moderate-resolution mixed-pixel reflectance by an LAI retrieval model under the assumption that the whole pixel is covered by biome type bio_$i$. Furthermore, the leaf angle distribution of the same biome type is usually assumed to be invariant in the LAI retrieval model [17]. Based on this, we assume that the foliage projection coefficient of biome type bio_$i$ used in an LAI retrieval model [$G_{\text{model\_bio\_}i}(\theta)$] is the same as the foliage projection coefficient of subpixels of biome type bio_$i$ [i.e., $G_{\text{model\_bio\_}i}(\theta) = G_i(\theta)$]; then, (3) can be simplified as

$$\text{MPCF} = \frac{\ln P_{\text{model\_a}}(\theta)}{\frac{1}{n}\sum_{i=1}^{n}\frac{\ln P_i(\theta)}{\frac{G_i(\theta)}{G_{\text{model\_a}}(\theta)}\frac{G_{\text{model\_a}}(\theta)}{G_{\text{model\_bio\_}i}(\theta)}\frac{L_{\text{model\_a}}}{L_{\text{model\_bio\_}i}}\frac{\ln P_{\text{model\_bio\_}i}(\theta)}{\ln P_{\text{model\_a}}(\theta)}}}$$

$$= \frac{L_{\text{model\_a}}}{\frac{1}{n}\sum_{i=1}^{n}\frac{\ln P_i(\theta)}{\ln P_{\text{model\_bio\_}i}(\theta)}L_{\text{model\_bio\_}i}}. \tag{5}$$

Thus, $L_m$ in (1) can be expressed as

$$L_m = \frac{L_{\text{model\_a}}}{\text{MPCF}} = \frac{L_{\text{model\_a}}}{\frac{L_{\text{model\_a}}}{\frac{1}{n}\sum_{i=1}^{n}\frac{\ln P_i(\theta)}{\ln P_{\text{model\_bio\_}i}(\theta)}L_{\text{model\_bio\_}i}}}$$

$$= \frac{1}{n}\sum_{i=1}^{n}\frac{\ln P_i(\theta)}{\ln P_{\text{model\_bio\_}i}(\theta)}L_{\text{model\_bio\_}i} \tag{6}$$

where $P_i(\theta)$ in (6) can be calculated based on a high-resolution FVC product using the following equation:

$$P_i(\theta) = 1 - \text{FVC}_i(\theta) \tag{7}$$

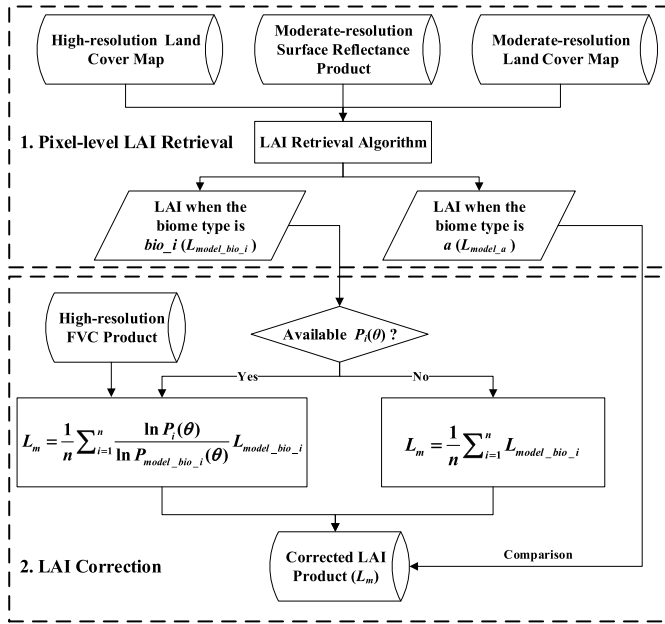where $\text{FVC}_i(\theta)$ is the FVC of subpixel $i$.

Fig. 1.    Framework of the MPC method.

In the retrieval of global moderate-resolution LAI products, it is difficult to obtain high-resolution gap proportions or FVC information at the global scale. Therefore, we further simplify (6) to address such a situation. Since the growth status of the same biome type is usually similar within a moderate-resolution pixel, we assume that the gap proportions of biome type bio_$i$ used in an LAI retrieval model $[P_{\text{model\_bio}\_i}(\theta)]$ are similar to the gap proportion of subpixels of biome type bio_$i$ [i.e., $P_{\text{model\_bio}\_i}(\theta) \approx P_i(\theta)$] when the MPC method is applied for retrieving the global LAI product. Then, (6) can be simplified as

$$L_m = \frac{1}{n}\sum_{i=1}^{n} L_{\text{model\_bio}\_i} = \sum_{\text{bio}\_i=1}^{n_b} \omega_i L_{\text{model\_bio}\_i} \qquad (8)$$

where $n_b$ is the number of biome types in the mixed pixel. $\omega_i$ is the area fraction of bio_$i$ in the mixed pixel. The high-resolution global land cover map is the only additional information required in the correction of the current moderate-resolution global LAI product when using (8). Based on the definition of the MPCF, the equation for retrieving $L_m$ can be converted from "the arithmetic average of the subpixel LAI (i.e., $L_i$)" to the "weighted average of $L_{\text{model\_bio}\_i}$." It is much more straightforward to estimate $L_{\text{model\_bio}\_i}$ than $L_i$ in the retrieval of $L_m$.

Fig. 1 shows the flowchart of the MPC method, including two main steps: 1) pixel-level LAI ($L_{\text{model\_a}}$ and $L_{\text{model\_bio}\_i}$) retrieval and 2) LAI correction. First, the biome combination within a moderate-resolution pixel is summarized based on the high-resolution data. Then, $L_{\text{model\_bio}\_i}$ and $P_{\text{model\_bio}\_i}(\theta)$ can be calculated based on the LAI retrieval algorithm using the reflectance data provided by the moderate-resolution surface reflectance products and the biome types provided by the high-resolution land cover maps within a moderate-resolution

pixel. When high-resolution gap proportion information is available, $L_m$ can be calculated using (6). $P_i(\theta)$ in (6) can be calculated based on the high-resolution FVC products using (7). When high-resolution gap information is not available, $L_m$ can be calculated using (8). Finally, $L_{\text{model\_a}}$ calculated based on the moderate-resolution surface reflectance products and land cover maps is compared with the LAI corrected by the MPC method ($L_m$) to evaluate the performance of the MPC method.

In this article, to evaluate its performance, the MPC method is used to correct the LAI retrieved by the main algorithm of the MODIS LAI product [16], which is formulated based on a 3-D radiative transfer (3DRT) model [17]. Scenes simulated by the DART model are used to assess the performance of the proposed MPC method when gap proportion information is available (i.e., (6) is used in the MPC method). In comparison, the aggregated 30-m Landsat LAI and site-based high-resolution LAI reference maps are used to assess the performance of the proposed MPC method when no high-resolution gap proportion information is available (i.e., (8) is used in the MPC method).

## III. DATA AND METHOD

### A. DART Simulation Data

DART, a 3DRT model developed at the Center for the Study of the Biosphere from Space (CESBIO) since 1993 [55], [56], is one of the most comprehensive radiative transfer models. It can be used to simulate the radiation budget and remotely sensed images of natural vegetation and artificial surfaces with topography and atmospheric effects. This model has been widely used in various remote sensing applications, such as the retrieval of remote sensing images [57], [58] and the study of the relationships between vegetation structures and satellite images [59]. The accuracy of the DART model in simulating the directional reflectance of the vegetation canopy has been extensively assessed with ground/airborne measurements [60] and model intercomparisons in the radiation transfer model intercomparison (RAMI) project [61]. Thus, we selected the DART model to simulate various scenes mixed with different biome types to evaluate the performance of the MPC method.

In this study, scenes of forest-grass, forest-crop, and crop-grass ecotones and scenes covered by the same biome type and LAI but with different distributions of vegetation cover were simulated using the DART model. The size of each scene was set to 100 m × 100 m, composed of 100 subpixels (10 m × 10 m) with no topography. The LAI values of deciduous broadleaf forests (DBFs), grasses, and crops in the simulated transition zones were set based on the following three principles.

1) The LAI retrieved by the MODIS main algorithm was valid (not a filled value) and exhibited little difference from the DART-simulated LAI when the scene was covered by one vegetation type and the vegetation was relatively homogeneously distributed in the scene to reduce the influence of the retrieval algorithm on the MPC method since the MPC method was not designed to correct the uncertainties caused by the retrieval algorithm.
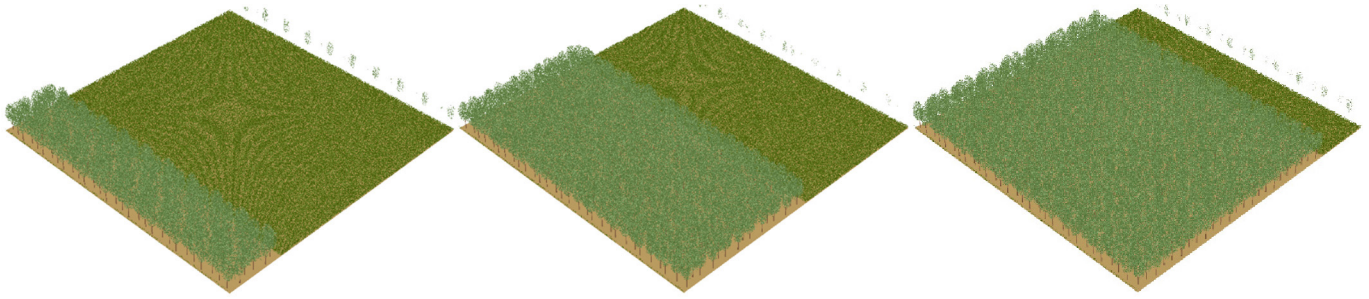
Fig. 2. Scenes of forest-grass transition zones simulated by the DART model with (Left) 20%, (Middle) 50%, and (Right) 80% DBFs.
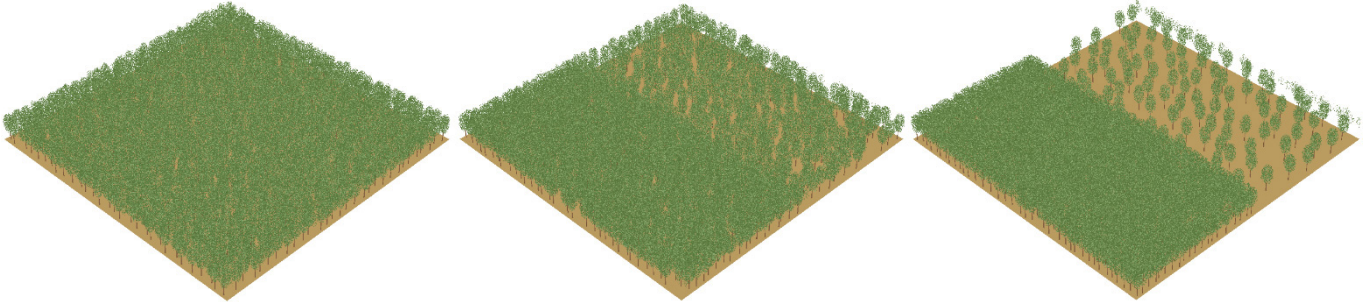


Fig. 3. Scenes covered by DBFs had the same LAI but different distributions of vegetation cover. The LAI value of the DBF in each entire scene was 3.0. The LAI values of the DBF in the left half of each scene were [from (Left) to (Right)] 3.0, 4.2, and 5.4, and the LAI values of the DBF in the right half of each scene were 3.0, 1.8, and 0.6.

2) The LAI of DBFs should be larger than that of grasses since such mixed scenes are more widely distributed worldwide.

3) The LAI of crops represented an early growth stage to highlight a relatively strong feature of row sowing crops to ensure that crop features were explicitly distinct from grass features. The LAI value of crops in the early growth stage partly refers to the LAI (0.95 for scenes with 0.8 m distance between rows) in [62].

Finally, the LAI values of DBFs, grasses, and crops in the simulated transition zones were set to 3.0, 2.0, and 1.2, respectively. The DBFs were simulated by the "Earth scene: Trees" module in the DART model. The trees had the same height and shape with an ellipsoidal crown shape. The tree leaves were assigned a spectrum of type "leaf_deciduous" from the DART database, with a spherical leaf angle distribution. The grasses were simulated by the "Earth scene: Plots" module in the DART model. The leaves of grasses were assigned a spectrum of type "grass_rye" from the DART database, with an erectophile leaf angle distribution. The crops were simulated by the "Earth scene: 3D imported object" module based on the 3-D object of maize in the DART model. The leaves of crops were assigned a spectrum of type "maize" from the DART database with an erectophile leaf angle distribution.

The proportions of DBFs, grasses, and crops varied from 0% to 100% with an increment of 10% in these simulated transition zones. Fig. 2 shows the scenes of forest-grass transition zones with 20%, 50%, and 80% DBFs. For the scenes covered by the same biome type, the LAI values of the entire scenes were fixed at 3.0, 2.0, and 1.2 for the scenes

covered by DBFs, grasses, and crops, respectively. To increase the heterogeneity of a scene, the LAI in half of the scene was increased, and the LAI in the other half of the scene was decreased. Fig. 3 shows the scenes covered by the DBF with the same LAI but different distributions of vegetation cover. Ultimately, 44 groups of scenes were generated based on the DART model.

### B. Land Cover Maps

*1) Finer Resolution Observation and Monitoring of the Global Land Cover Dataset:* In this study, the 2015 Finer Resolution Observation and Monitoring of Global Land Cover (FROM-GLC) map [63], [64], [65] with a resolution of 30 m was used to provide the high-resolution land cover information employed to evaluate the MPC method based on the high-resolution LAI maps retrieved from the Landsat-8 reflectance products. FROM-GLC includes ten classes and 26 subclasses with an overall accuracy of >71%. The classification scheme of FROM-GLC is reclassified into the MODIS LAI/fraction of photosynthetically active radiation (FPAR) biome classification scheme described by Myneni et al. [16]. The relationship between the FROM-GLC classification scheme and the LAI biome classification scheme is shown in Table I. The former scheme does not contain a class corresponding to savannas in the latter scheme, probably because savannas are, by definition, a mixed class of forests, shrubs, and grasses and, thus, can be classified as forests, shrubs, or grasses on the 30-m scale.

*2) MODIS Land Cover Type Product:* The MODIS land cover type product (MCD12Q1) was derived based on a

| FROM-GLC | | LAI classes | |
|---|---|---|---|
| Value | Classes | Value | Classes |
| 10 | Cropland | 3 | Broadleaf Croplands |
| 21 | Broadleaf, leaf-on | 5 | Evergreen Broadleaf Forests |
| 22 | Broadleaf, leaf-off | 6 | Deciduous Broadleaf Forests |
| 23 | Needleleaf, leaf-on | 7 | Evergreen Needleleaf Forests |
| 24 | Needleleaf, leaf-off | 8 | Deciduous Needleleaf Forests |
| 30 | Grassland | 1 | Grasslands |
| 40 | Shrublands | 2 | Shrublands |
| 50 | Wetland | 1 | Grasslands |
| 60 | Water | 0 | Water Bodies |
| 71 | Shrub and brush tundra | 2 | Shrublands |
| 72 | Herbaceous tundra | 1 | Grasslands |
| 80 | Impervious surface | 10 | Urban and Built-up Lands |
| 90 | Bareland | 9 | Non-Vegetated Lands |
| 100 | Snow/Ice | 9 | Non-Vegetated Lands |
| 120 | Cloud | 255 | Unclassified |

supervised decision tree classification method from MODIS observations spanning an entire year [66]. The MCD12Q1 product includes five land cover classification schemes. Among them, the LAI/FPAR biome classification scheme described by Myneni et al. [16] is used to provide moderate-resolution biome type information for an evaluation of the MPC method based on the aggregated 30-m Landsat LAI and site-based high-resolution LAI reference maps.

### C. Landsat-8 Reflectance Products

The Landsat-8 reflectance products used in this study were downloaded from the website of the United States Geological Survey (USGS) Earth Resources Observation and Science (EROS) Center (https://espa.cr.usgs.gov/). The reflectance products were atmospherically corrected using the Second Simulation of a Satellite Signal in the Solar Spectrum (6S) tools [67].

In this study, Landsat-8 reflectance products and their corresponding view and illumination angles were used to produce high-resolution LAI data with the help of the reclassified FROM-GLC dataset based on the MODIS main algorithm. Two tiles (tiles 130-044 on May 3 and tiles 121-029 on July 7) of Landsat-8 reflectance data with less than 10% cloud cover in 2015 were utilized in this study. Tile 130-044 is in southwest China. The statistics based on the FROM-GLC maps at the MODIS pixel scale show that tile 130-044 is a forest-dominated tile covered by 22% pure evergreen broadleaf

forest (EBF), 39% forest-shrub-grass-crop transition zones, 23% forest-shrub-grass transition zones, 11% forest-grass transition zones, 3% forest-shrub transition zones, and 2% forest-grass-crop transition zones. Tile 121-029 is in northeastern China. It is a grass-dominated tile covered by 24% pure grasslands, 26% grass-forest-crop transition zones, 25% grass-crop transition zones, 20% grass-forest transition zones, 3% grass-forest-shrub-crop transition zones, 1% grass-shrub-crop transition zones, and 1% grass-forest-shrub transition zones.

### D. Field-Measured LAI and Site-Based LAI Reference Maps From the VALERI Database

To validate the accuracy of the MPC method, we collected the LAI at 14 sites measured in the Validation of Land European Remote Sensing Instruments (VALERI) project (http://w3.avignon.inra.fr/valeri). Detailed information on these 14 sites is shown in Table II. The LAI data were processed from hemispherical images of each elementary sampling unit (ESU) using CAN-EYE software. Each site contained between 30 and 100 ESUs. High-resolution LAI reference maps with a spatial resolution of 20 m were generated based on a transfer function derived from high-resolution SPOT/Landsat reflectance products, land cover maps, and LAI field measurements. These reference maps have been widely used in various studies to validate LAI products [27], [28], [29], [34], [36], [37], [38], [39].

### E. Evaluation Strategy of the MPC Method

To assess the performance of the MPC method, the LAI retrieved by the MODIS main algorithm (termed the MOD LAI) was compared with the LAI retrieved after the correction of the MPC method based on the DART-simulated LAI, aggregated Landsat LAI, and site-based high-resolution LAI reference maps. The LAI retrieved by the MPC method using (6) with the FVC information is referred to as the MPC_F LAI. The LAI retrieved by the MPC method using (8) without the FVC information is referred to as the MPC LAI. The details are shown in the following.

*1) Assessment of the MPC Method Based on DART Simulations:* The LAI values of the scenes set in the DART model were regarded as the reference LAI values to assess the performance of the MPC method.

For the scenes with transition zones, the two biome types in the scenes were used separately as the input biome types in the MODIS main algorithm to generate two groups of LAI values based on the DART-simulated angular reflectance in the red and near-infrared bands. Then, these groups of LAI values were corrected by the MPC method based on the biome type and gap proportion of the $10 \times 10$ subpixels in the scene. The results obtained by the MODIS main algorithm using the dominant biome type were used to evaluate the performance of the MPC method for mixed land cover types, whereas the results retrieved by the MODIS main algorithm using the nondominant biome type were used to evaluate the performance of the MPC method for biome misclassification.

For the scenes covered by a single biome type but with different distributions of vegetation cover, the MOD LAI

TABLE II

CHARACTERISTICS OF THE 14 VALERI VALIDATION SITES. "DATE OF MODIS PRODUCT" REPRESENTS THE OBSERVATION DATES OF THE MOD09GA AND/OR MYD09GA PRODUCTS USED IN THE LAI RETRIEVAL BASED ON THE MODIS MAIN ALGORITHM AND THE MPC METHOD

| ID | Location | | | Latitude | Longitude | Main Biome Type | Date of Measurement | | Date of MODIS Product | |
|---|---|---|---|---|---|---|---|---|---|---|
| | Continent | Country | Site | | | | Year | DOY | Year | DOY |
| 1 | Africa | Benin | Donga | 9.83 | 1.61 | Grasslands | 2005 | 171 | 2005 | 169-176 |
| 2 | Asia | China | Zhangbei | 41.28 | 114.69 | Pastures | 2002 | 221 | 2002 | 217-224 |
| 3 | Europe | Belgium | Sonian_forest | 50.77 | 4.41 | Forests | 2004 | 174 | 2004 | 169-176 |
| 4 | | France | Le_Larzac | 43.94 | 3.12 | Grasslands | 2002 | 203 | 2002 | 201-208 |
| 5 | | | Les_Alpilles | 43.81 | 4.71 | Crops | 2002 | 204 | 2002 | 201-208 |
| 6 | | | Plan-de-Dieu | 44.20 | 4.95 | Crops | 2004 | 189 | 2004 | 185-192 |
| 7 | | | Sud-Ouest | 43.51 | 1.24 | Crops | 2002 | 189 | 2002 | 185-192 |
| 8 | | Germany | Demmin | 53.89 | 13.19 | Crops | 2004 | 164 | 2004 | 161-168 |
| 9 | | Romania | Fundulea | 44.41 | 26.58 | Crops | 2001 | 128 | 2001 | 121-128 |
| | | | | | | | 2002 | 144 | 2002 | 137-144 |
| | | | | | | | 2003 | 144 | 2003 | 137-144 |
| 10 | | Spain | Barrax | 39.07 | -2.13 | Crops | 2003 | 196 | 2003 | 193-200 |
| 11 | North America | Canada | Larose | 45.38 | -75.22 | Mixed Forests | 2003 | 219 | 2003 | 217-224 |
| 12 | Oceania | Australia | Camerons | -32.59 | 116.25 | Broadleaf Forests | 2004 | 63 | 2004 | 57-64 |
| 13 | | | Gnangara | -31.53 | 115.87 | Broadleaf Forests | 2004 | 61 | 2004 | 57-64 |
| 14 | South America | French Guiana | Counami | 5.36 | -53.24 | Tropical Forests | 2001 | 269 | 2001 | 265-272 |
| | | | | | | | 2002 | 286 | 2002 | 281-288 |

values were compared with the MPC LAI values to evaluate the performance of the MPC method in reducing the effect of the density variation of vegetation cover. The standard deviation (SD) of FVC was used as a quantitative indicator to capture the intensity of the heterogeneity level. The larger the SD of FVC is, the stronger the heterogeneity.

*2) Evaluation of the MPC Method Based on the Aggregated Landsat LAI:* The high-resolution LAI maps retrieved from the Landsat-8 reflectance products and FROM-GLC data based on the MODIS main algorithm were regarded as the reference LAI values to evaluate the performance of the MPC method. The Landsat-8 reflectance products and FROM-GLC data were projected onto the sinusoidal projection used in the MCD12Q1 product to reduce the errors caused by resampling. The moderate-resolution LAI values were generated using the MODIS main algorithm based on the moderate-resolution land cover data obtained from the MCD12Q1 product and the aggregated Landsat-8 reflectance data using the arithmetic average method. Then, the generated LAI values were corrected by the MPC method with the help of the FROM-GLC data. Finally, the moderate-resolution MOD LAI or MPC LAI values were compared with the arithmetic average of the Landsat LAI under different dominant vegetation type percentages (DVTPs) [68] to explore the influences of mixed land cover types and biome misclassification on the LAI retrievals.

The DVTP used in this article was defined as the proportion of the dominant vegetation type in a moderate-resolution pixel [68].

*3) Validation of the MPC Method Based on Site-Based LAI Reference Maps:* Site-based high-resolution LAI maps aggregated at the MODIS pixel scale were compared with the moderate-resolution MOD LAI or MPC LAI values to evaluate the performance of the MPC method. First, the daily moderate-resolution LAI values at the validation sites were retrieved by the MODIS main algorithm based on the MCD12Q1 product and MODIS daily reflectance data listed in Table II. Then, the LAI retrievals were corrected by the MPC method based on the high-resolution land cover maps used in the generation of high-resolution LAI reference maps provided by the corresponding VALERI sites. The daily MOD LAI and MPC LAI were composited into the eight-day LAI using a compositing algorithm based on the maximum FPAR [16]. High-quality eight-day composited MOD LAI and MPC LAI retrievals, which were not contaminated by clouds, cloud shadows, or snow, were then compared with the aggregated LAI reference maps. Note that, since the MPC method was proposed to improve the accuracy of LAI retrievals for mixed pixels, the results were used only when DVTP < 0.9 to ensure pixel heterogeneity [51]. Finally, a total of 874 available pixels were used to validate the MPC method.
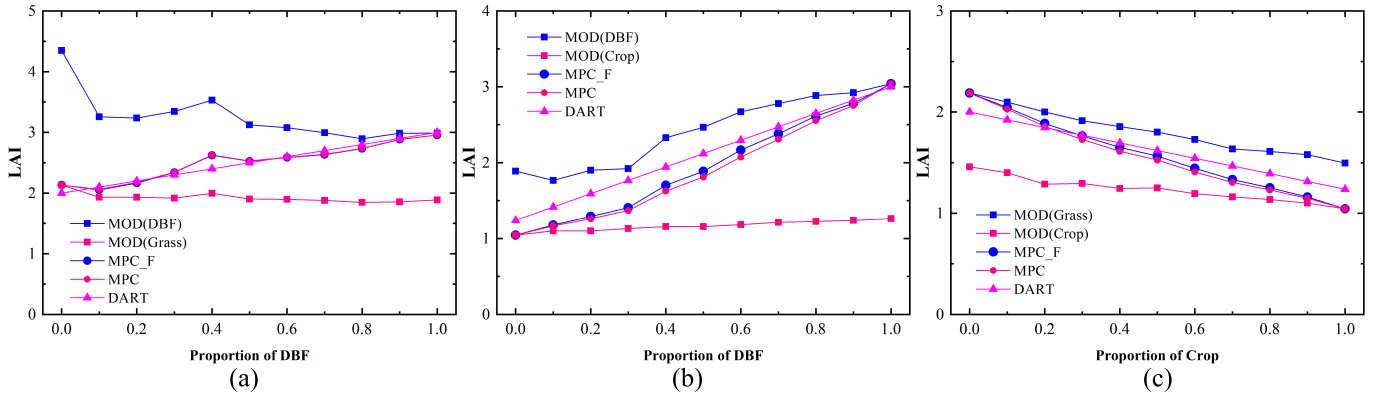
Fig. 4.   Comparison of the LAI values retrieved using the MODIS main algorithm (MOD LAI) with the LAI values corrected by the MPC method based on the DART-simulated LAI for (a) forest-grass, (b) forest-crop, and (c) crop-grass transition zone scenes. The biome type in the bracket represents the input moderate-resolution biome type in the MODIS main algorithm. The LAI retrieved by the MPC method using (6) with the FVC information is referred to as MPC_F LAI. The LAI retrieved by the MPC method using (8) without the FVC information is referred to as MPC LAI.

*4) Influence of Mixed Land Cover Types at the Global Scale Based on the FROM-GLC Dataset:* The 30-m FROM-GLC dataset was compared with the MCD12Q1 product in 2015 to show the need to consider land cover mixtures on LAI retrievals at the global scale. First, the FROM-GLC classification scheme was reclassified into the LAI biome classification scheme used in the MCD12Q1 product based on the relationship shown in Table I. Then, the FROM-GLC dataset was projected to the sinusoidal projection of the MCD12Q1 product to reduce the sampling errors. One MODIS pixel contained $15 \times 15$ converted FROM-GLC pixels. Finally, the global spatial distribution of the number of vegetation biome types on the MODIS pixel scale ($\sim$500 m) was summarized based on the 30-m FROM-GLC maps in 2015 to explore the necessity of the MPC method.

## IV. RESULTS

### A. Assessment of the MPC Method Based on DART Simulations

*1) Results of Scenes Mixed With Different Biome Types:* Fig. 4 compares the LAI retrieved using the MODIS main algorithm with the LAI corrected by the MPC method based on the DART-simulated LAI for scenes of forest-grass, forest-crop, and crop-grass transition zones. As shown in Fig. 4, when the dominant biome type was used as the input biome type in the MODIS main algorithm and DVTP $\geq$ 90%, the MOD LAI was similar to both the DART-simulated LAI and the LAI retrieved by the MPC method. In contrast, as shown in Fig. 4(a) and (b), when the dominant biome type was used as the input biome type in the MODIS main algorithm and DVTP < 90%, the MODIS main algorithm overestimated the DART-simulated LAI for forest (DBF)-dominated scenes mixed with herbaceous vegetation (grasses or crops), and the magnitude of overestimation increased with decreasing DVTP. In comparison, the MODIS main algorithm underestimated the DART-simulated LAI for herbaceous vegetation-dominated scenes mixed with forests, and the magnitude of underestimation similarly increased with decreasing DVTP. The MPC method can reduce the influence of such mixed land

cover types to obtain a more accurate LAI than that obtained by the MODIS main algorithm. For scenes of crop-grass transition zones, the MPC LAI results were also slightly more in accordance with the DART-simulated LAI than were the MOD LAI.

The FVCs for scenes covered by homogenous DBF, grass, and crop were 0.5529, 0.5532, and 0.4716, respectively. For scenes of forest-grass transition zones [see Fig. 4(a)], the MPC_F LAI was very similar to the MPC LAI, probably because the SD of FVC (i.e., the degree of spatial heterogeneity) of these scenes was very small. For scenes of forest-crop and crop-grass transition zones [see Fig. 4(b) and (c)], the MPC_F LAI was closer to the DART LAI with slightly larger LAI values than the MPC LAI. The difference between MPC_F and MPC LAI increased with increasing spatial heterogeneity.

As shown in (8), the MPC LAI values are determined mainly by the input high-resolution land cover maps and are not sensitive to the input moderate-resolution biome type. Note that the MPC method still slightly underestimated the DART-simulated LAI for the crop-dominated scenes, probably because the MODIS main algorithm underestimated the DART-simulated LAI when the scene was covered by homogenous pure crops. The MPC method cannot correct uncertainties caused by the retrieval algorithm since it was developed primarily to reduce the effects of mixed land cover types and biome misclassification.

When the nondominant biome type was used as the input biome type in the MODIS main algorithm, large errors were found for all transition zone scenes (see Fig. 4), especially for the forest-grass transition zone scenes. The MOD LAI retrievals were overestimated when the biome type of herbaceous vegetation was misclassified into the biome type of forests or when the biome type of crops was misclassified into the biome type of grasses. The MOD LAI retrievals were underestimated when the biome type of forests was misclassified into the biome type of herbaceous vegetation or when the biome type of grasses was misclassified into the biome type of crops. In comparison, the MPC method can reduce the errors caused by biome misclassification to obtain
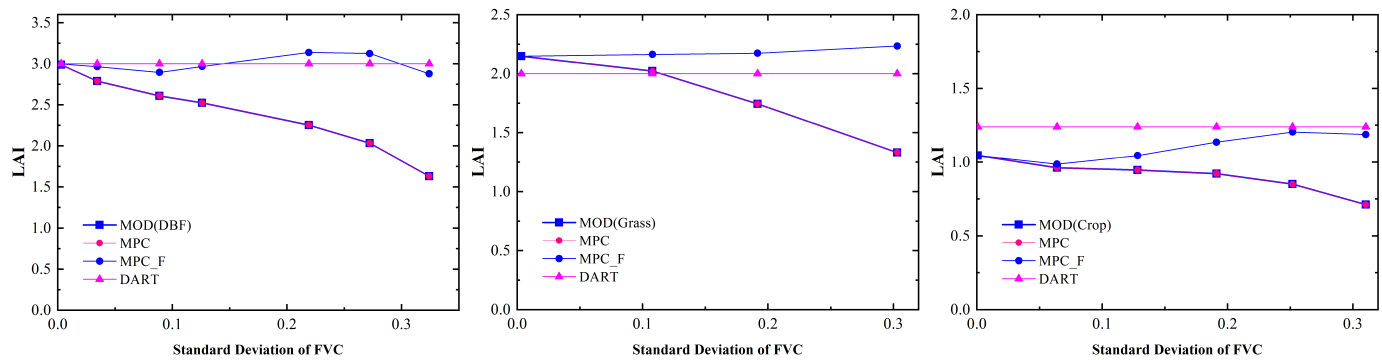
Fig. 5. Variations in MOD LAI, MPC LAI, MPC_F LAI, and DART-simulated LAI with an increase in the SD of the FVC for scenes covered by a single biome type with different degrees of spatial heterogeneity. The biome type in the bracket represents the input moderate-resolution biome type in the MODIS main algorithm.

a more accurate LAI, given that the high-resolution land cover map was accurate.

In summary, the MPC method can reduce the effects of mixed land cover types and biome misclassification in the retrieval of moderate-resolution LAI.

*2) Results of Scenes Covered by a Single Biome Type With Different Degrees of Spatial Heterogeneity:* In this section, the MOD LAI retrievals are compared with the LAI retrieved by the MPC method based on DART-simulated scenes covered by a single biome type with different degrees of spatial heterogeneity (see Fig. 5). As shown in Fig. 5, the MOD LAI decreases with an increase in the SD of the FVC for scenes covered by a single biome type. This result is consistent with the results proposed by Yin et al. [51]. The MPC LAI values without considering the FVC information are the same as the MOD LAI. In comparison, the MPC method can reduce the influence of heterogeneity caused by the density variation of vegetation cover to obtain a more stable LAI (i.e., MPC_F LAI) with the help of high-resolution FVC information of the scene. In addition, the MPC_F LAI values are similar to the MOD LAI retrievals when the scenes are relatively homogenous. Thus, the accuracy of the MPC_F LAI depends largely on the accuracy of the MOD LAI for homogenous scenes since the MPC method cannot correct the uncertainties caused by the retrieval algorithm.

*B. Evaluation of the MPC Method Based on the Aggregated Landsat LAI*

*1) Performance of the MPC Method for Mixed Land Cover Types:* Fig. 6 shows scatterplots that compare the aggregated 30-m Landsat LAI with the MOD and MPC LAI retrievals for forest-dominated tile 130-044 on May 3, 2015, and grass-dominated tile 121-029 on July 7, 2015. The dominant land cover types and corresponding DVTPs at the MODIS pixel scale are calculated based on the 30-m FROM-GLC maps. The dominant land cover types for the pixels shown in Fig. 6 are the same as the land cover types in the MCD12Q1 product and are used as the input biome types in the MODIS main algorithm and the MPC method. Of the pixels shown in Fig. 6(a) and (b), 94.4% are dominated by EBF, and of the pixels shown in Fig. 6(c) and (d), 98.7% are dominated by grasslands.

As shown in Fig. 6, the MOD LAI retrievals are similar to the MPC LAI retrievals for the relatively homogenous pixels (DVTP ≥ 0.9). For heterogeneous pixels mixed with different biome types (DVTP < 0.9), the MODIS main algorithm overestimates the aggregated Landsat LAI for forest-dominated pixels [see Fig. 6(b)], especially for forest-dominated pixels mixed with a large proportion of herbaceous vegetation. The LAI overestimation can reach a maximum of 2.673 (69.8%) for a pixel covered by 50.2% forests, 42.2% grasslands, and 7.6% shrubs (termed Pixel A in the remainder of this article). In contrast, the MODIS main algorithm underestimates the aggregated Landsat LAI for the grass-dominated pixels mixed with a large proportion of forests and slightly overestimates the aggregated Landsat LAI for the grass-dominated pixels mixed with croplands [see Fig. 6(d)]. The LAI underestimation can reach a maximum of 1.313 (53.3%) for a pixel covered by 56.9% grasslands and 43.1% forests (termed Pixel B in the remainder of this article). The MPC method can reduce the effect of mixed land cover types to obtain a more accurate LAI with a much smaller RMSE and higher R2 than the MODIS main algorithm. The RMSE (its relative value) decreases by 0.198 (49.0%) for the forest-dominated tile [see Fig. 6(b)] and by 0.121 (63.0%) for the grass-dominated tile [see Fig. 6(d)]. The absolute errors [relative errors (REs)] of the MPC LAI are reduced to 0.384 (10.0%) for Pixel A and to 0.221 (9.0%) for Pixel B.

The RMSE and RE between the MOD or MPC LAI retrievals and the aggregated Landsat LAI under different DVTPs are also calculated for the EBF-dominated and grass-dominated pixels (see Fig. 7). The RMSE of the MOD LAI increases rapidly with decreasing DVTP due to the enhancement of the land cover mixing effect, which is consistent with the results proposed by Tian et al. [44]. In comparison, the MPC method can reduce the effect of mixed land cover types, thereby achieving more accurate LAI retrievals with much smaller RMSE and RE values.

In summary, the MPC method can still reduce the influence of mixed land cover types to obtain a more accurate LAI than that of the MODIS main algorithm when no high-resolution gap proportion information is available.

*2) Performance of the MPC Method for Biome Misclassification:* Fig. 8 shows scatterplots that compare the aggregated
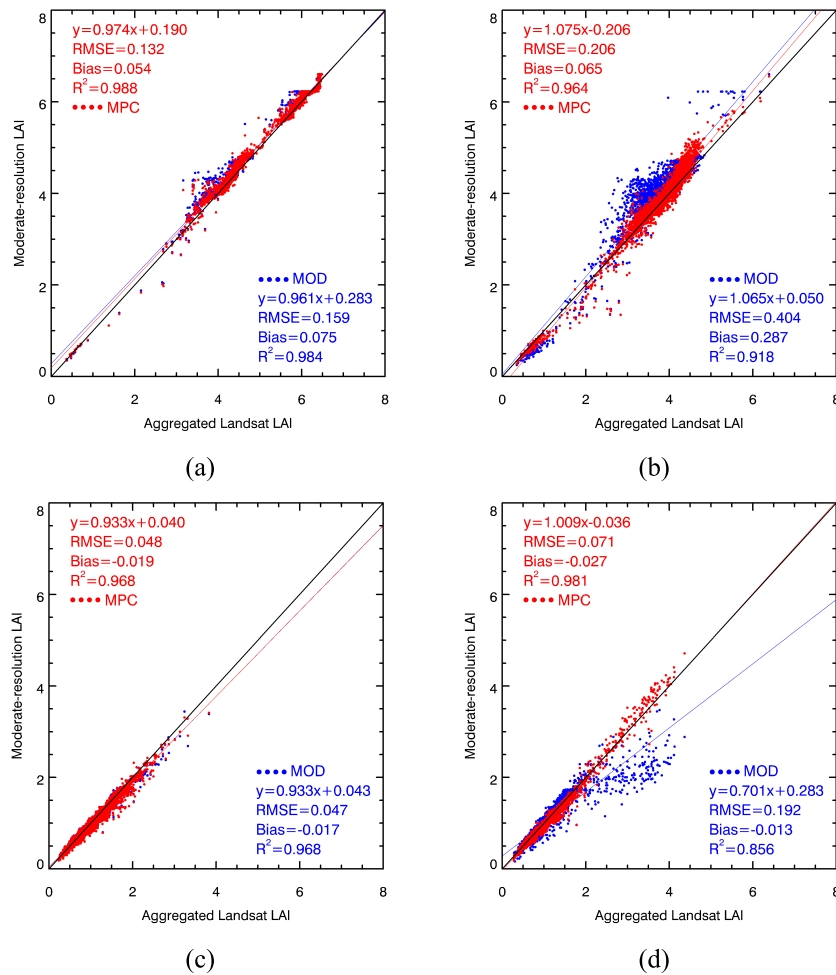
Fig. 6. Comparison of the aggregated Landsat LAI with the MOD (blue dots) and MPC (red dots) LAI for forest-dominated tile 130-044 (a) and (b) on May 3, 2015, and grass-dominated tile 121-029 (c) and (d) on July 7, 2015, when the dominant biome types of pixels calculated based on the FROM-GLC data are the same as the biome types in the MCD12Q1 product. The blue and red lines are the regression lines of MOD and MPC LAI, respectively. The black line is the 1:1 line (i.e., $y = x$). (a) DVTP $\geq$ 0.9 (forest-dominated). (b) DVTP < 0.9 (forest-dominated). (c) DVTP $\geq$ 0.9 (grass-dominated). (d) DVTP < 0.9 (grass-dominated).
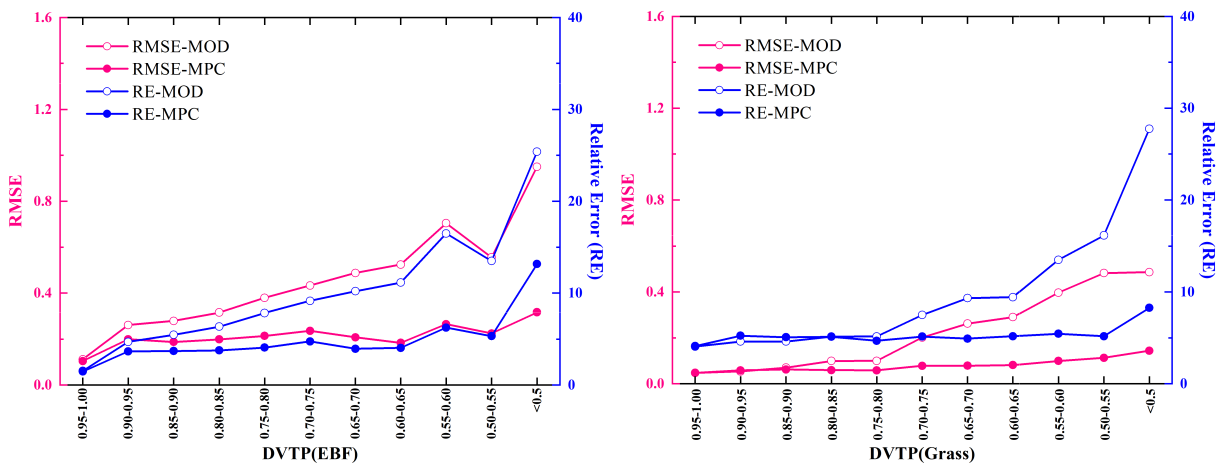


Fig. 7. Variations in the RMSE and RE between the MOD or MPC LAI retrievals and the aggregated Landsat LAI with decreasing DVTP for [(Left) 130-044] forest-dominated tile and [(Right) 121-029] grass-dominated tile.

30-m Landsat LAI with the MOD and MPC LAI retrievals for the forest-dominated tile and the grass-dominated tile when

the dominant biome types summarized from the FROM-GLC maps were different from the biome types in the MCD12Q1
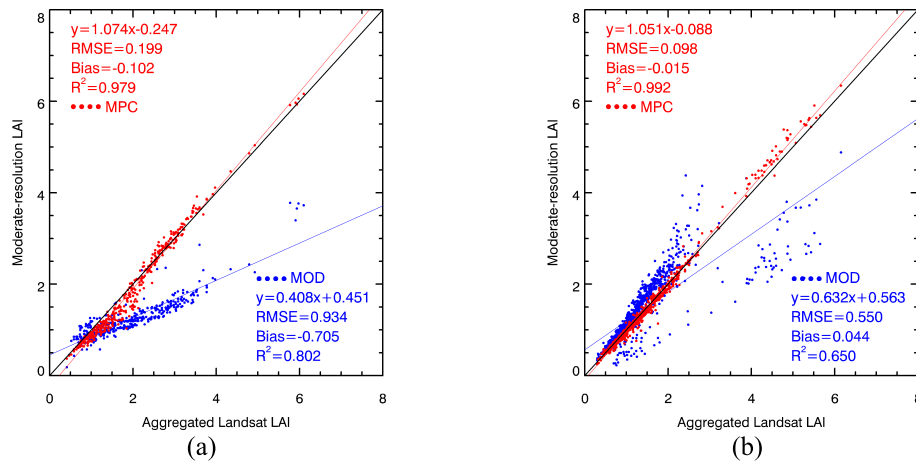
Fig. 8. Comparison of the aggregated Landsat LAI with the estimated LAI for forest-dominated tile 130-044 (a) on May 3, 2015, and grass-dominated tile 121-029 (b) on July 7, 2015, when the dominant biome types summarized from the FROM-GLC maps were different from the biome types in the MCD12Q1 product. (a) Forest-dominated. (b) Grass-dominated.
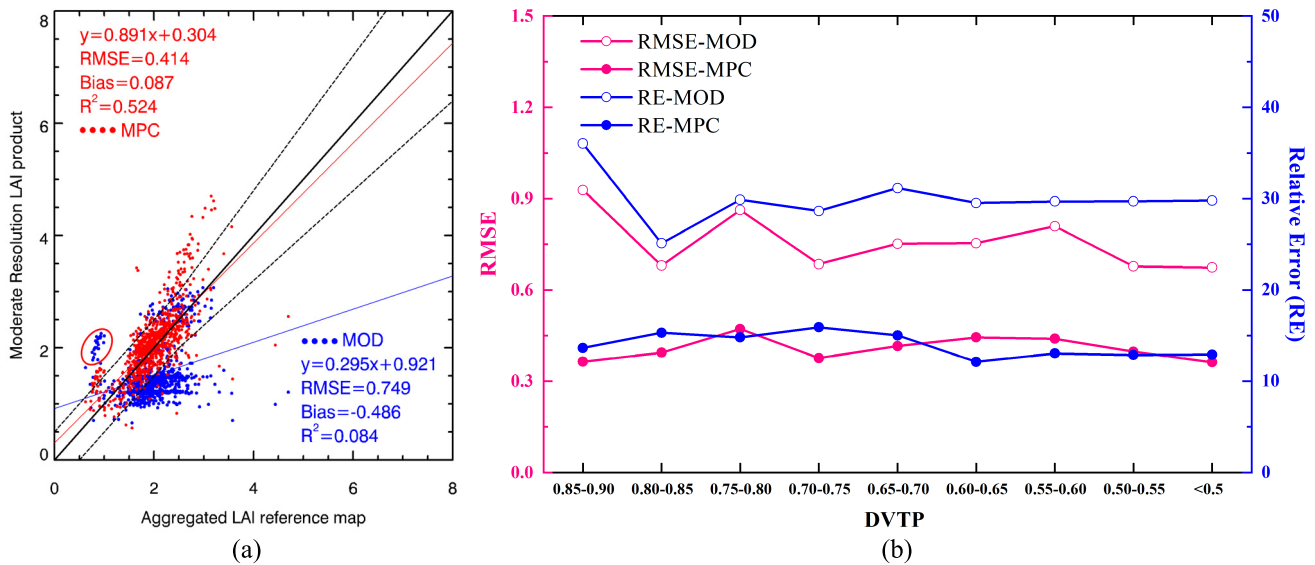


Fig. 9. Plots for (a) comparison of the site-based aggregated LAI reference maps with the MOD and MPC LAI retrievals for 14 validation sites and (b) variations in the RMSE and RE between the MOD or MPC LAI retrievals and the aggregated LAI reference maps in different DVTP intervals.

product (i.e., when the nondominant biome types were used as the input moderate-resolution biome types in the MODIS main algorithm and the MPC method). As shown in Fig. 8, the MOD LAI deviated from the aggregated Landsat LAI when incorrect land cover types were used as the input biome types. The MODIS main algorithm underestimated the Landsat LAI when the forest-dominated pixels were misclassified into the biome types of grasslands, croplands, and savannas [see Fig. 8(a)]. In contrast, for the grass-dominated pixels, the MODIS main algorithm overestimated the Landsat LAI when those pixels were misclassified as savannas or forests and underestimated the Landsat LAI when those pixels were misclassified as croplands [see Fig. 8(b)]. In comparison, the MPC method can reduce the effect of biome misclassification to obtain a more accurate LAI with a much smaller RMSE and bias and a much higher R2.

## C. Validation of the MPC Method Based on Site-Based LAI Reference Maps

Fig. 9 shows the validation results from comparing the MOD LAI and MPC LAI with the site-based high-resolution LAI reference maps. Overall, the MOD LAI retrievals were underestimated compared with the aggregated reference LAI map except for the results marked by the red ellipse in Fig. 9(a), which corresponds to a grass-dominated site named Le_Larzac. The MODIS main algorithm overestimated the aggregated reference LAI at Le_Larzac, probably because the biome type used in the MODIS main algorithm was misclassified as savannas instead of grasslands, thus resulting in a great overestimation, which is in accordance with the finding of Fang et al. [47], which was that the "misclassification of savannas as any of the herbaceous types overestimates the
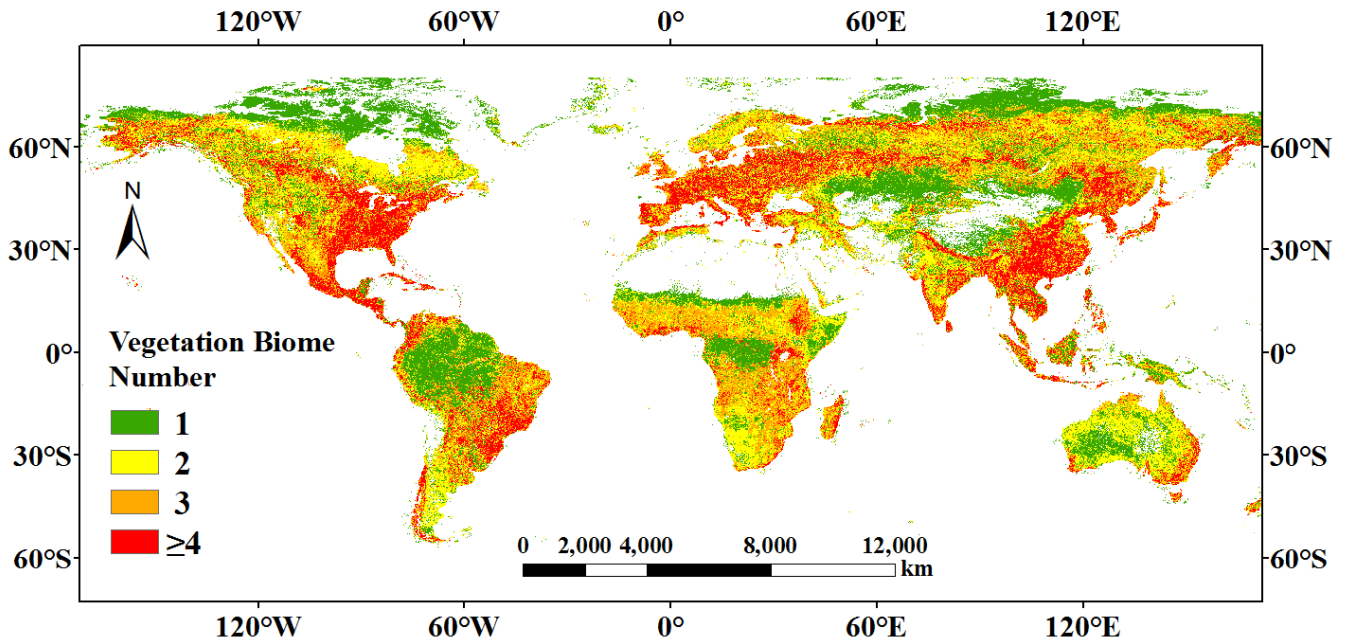
Fig. 10. Global spatial distribution of the number of vegetation biome types at the MODIS pixel (∼500 m) scale calculated based on the 30-m FROM-GLC maps in 2015.

LAI." In comparison, the MPC method can reduce the effects of mixed land cover types and biome misclassification to obtain a more accurate LAI than the MODIS main algorithm. The RMSE (bias) decreased from 0.749 (0.486) to 0.414 (0.087), while the R2 increased from 0.084 to 0.524, and the proportion of pixels that fulfilled the uncertainty requirement of the GCOS [<max(0.5, 20%)] increased from 38.2% to 84.6%. We further assessed the performance of the MPC method in different DVTP intervals, where each interval contained at least 23 available pixels. As shown in Fig. 9(b), the MPC LAI retrievals were much more consistent with the aggregated reference LAI than were the MOD LAI retrievals in all of the DVTP intervals.

### D. Influence of Mixed Land Cover Types at the Global Scale Based on the FROM-GLC Dataset

Fig. 10 shows the global spatial distribution of the number of vegetation biome types at the MODIS pixel scale (∼500 m) calculated based on the 30-m FROM-GLC maps in 2015. Multibiome mixed pixels are widely distributed worldwide. The proportion of multibiome mixed pixels for each biome was calculated based on the MCD12Q1 product [see Fig. 11(a)]. Pixels mixed with at least two biome types accounted for 75.5% of all vegetation-covered pixels. The biome type of savannas had the largest proportion of multibiome mixed pixels (95.0%) among all biome types, probably because, by definition, savannas are a mixed biome type in the LAI classification scheme (vegetation with 10%–60% tree cover). In contrast, the proportion of multibiome mixed pixels still reached 41.3% for the biome type of EBF, which had the smallest proportion of multibiome mixed pixels. Fig. 11(b) shows that the DVTP for 58.9% of vegetation-covered pixels was less than 0.9. Thus, as discussed in

Sections IV-A and IV-B, the heterogeneity of these pixels should be considered and reduced. In addition, nearly 27.5% of vegetation-covered pixels had very strong heterogeneity (DVTP < 0.6) which would result in large errors if no correction for mixed land cover types was applied. Such a large proportion of multibiome mixed pixels with strong heterogeneity highlights the need to consider the effect of mixed land cover types in the generation of global LAI products.

As shown in Fig. 11(c), there were more pixels worldwide composed of two mixed biome types than there were pixels consisting of any other number of biome types. We generated histograms for different biome type combinations [see Fig. 11(d)] and found that scenes of forest-grass transition zones were the most widely distributed among the pixels composed of two mixed biome types. As discussed in Sections IV-A and IV-B, the estimated LAI values in scenes of forest-grass transition zones are underestimated for pixels classified as grasslands and overestimated for pixels classified as forests without correcting for mixed land cover types. Therefore, it is essential to reduce the effect of mixed land cover types to obtain a more accurate LAI in the retrieval of moderate-resolution LAI products.

### V. DISCUSSION

### A. Influence of the Land Cover Maps on the MPC Method

As indicated in (6) and (8), the MPC LAI is not affected by the input moderate-resolution land cover product in the MODIS main algorithm and is instead determined by the high-resolution land cover data. When the input high-resolution land cover maps are accurate, the MPC method performs well in correcting the influence of biome misclassification (see Figs. 4 and 8). On the other hand, errors in these
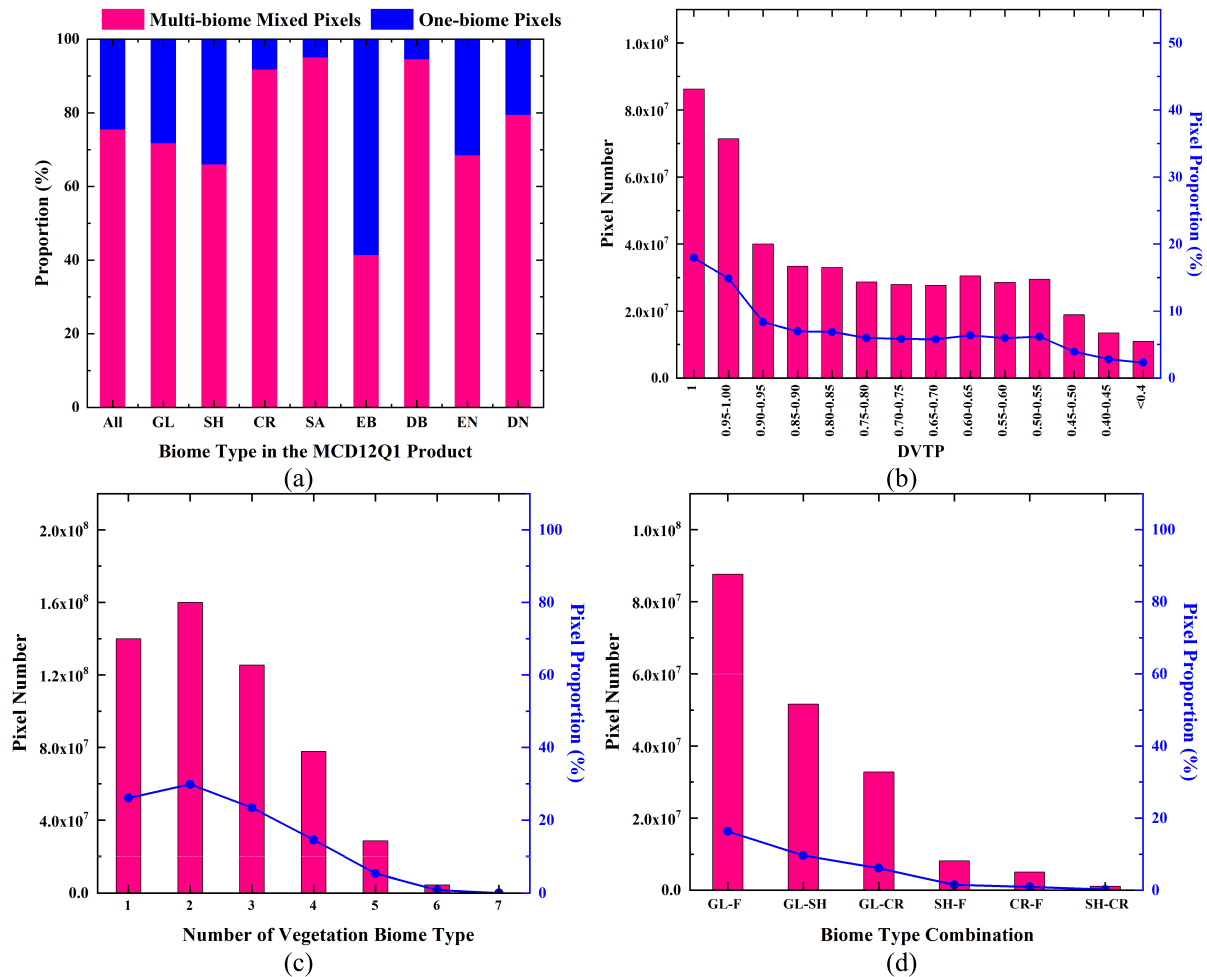
Fig. 11. (a) Proportion of multibiome mixed pixels for each biome type in the MCD12Q1 product. Histograms of (b) number (pink columns) and proportion (blue line) of pixels under different DVTPs, (c) number of pixels containing each number of vegetation biome types, and (d) biome type combinations for the global vegetation-covered moderate-resolution pixels calculated based on the FROM-GLC maps. The pixel proportion (blue line) is the ratio of the corresponding pixel number to the number of global vegetation pixels. GL, SH, CR, SA, EB, DB, EN, and DN represent the grassland, shrubland, cropland, savanna, evergreen broadleaf forest, deciduous broadleaf forest, evergreen needleleaf forest, and deciduous needleleaf forest biome types, respectively. All the biome types of forests (EB, DB, EN, and DN) are regarded as one biome type in the statistics of biome type combinations and are collectively referred to as F.

high-resolution land cover maps will completely transfer to the MPC LAI. Therefore, the accuracy of the high-resolution land cover maps has a great impact on the accuracy of the MPC LAI.

The eight vegetation types described in the LAI/FPAR biome classification scheme are used as the input biome types in the derivation of the 3DRT model. The CI value and the foliage projection coefficient of each biome type set in the 3DRT model are derived based on the principle that these parameters can well describe the clumping effect and leaf angle distribution in most cases when the pixels are relatively homogeneous. Therefore, the error caused by the assumption of an invariant CI value and foliage projection coefficient within the same biome type is relatively small when the high-resolution subpixels of the corresponding biome type described in the high-resolution land cover maps are homogenous. The error may be further reduced if a more detailed vegetation classification scheme (e.g., the classification scheme of FROM-GLC) is used in the derivation of the 3DRT model because the difference in CI values or

foliage projection coefficients within the same biome type will decrease as the number of classified vegetation types increases.

### B. Influence of High-Resolution Gap Proportion Information on the MPC Method

Spatial heterogeneity within pixels generally manifests in two ways: mixtures of different land cover types and density variations in vegetation cover [68], [69].

The gap proportion within the same biome type in a moderate-resolution pixel is assumed to be invariant when the MPC method is applied to correct the operational algorithms of global moderate-resolution LAI products. This assumption ignores the influence of heterogeneity caused by the density variation of vegetation cover. Therefore, the LAI after the correction of the MPC method may still underestimate the mixed-pixel LAI for pixels featuring a strong density variation in vegetation cover. Nevertheless, the results in Sections IV-B and IV-C demonstrate the accuracy of the MPC method even if the density variation of vegetation cover in a mixed pixel is

ignored, possibly because the number of pixels with a strong density variation of vegetation cover does not account for a large proportion of the mixed pixels corrected by the MPC method. The MPC method can still reduce the influences of mixed land cover types and biome misclassification based on high-resolution land cover maps to obtain more accurate LAI retrievals even if no high-resolution FVC data are available. Therefore, (8) can be used as a reasonable substitute instead of (6) when applying the MPC method to produce global moderate-resolution LAI products.

As indicated in Section IV-A, when high-resolution land cover maps and corresponding gap proportion information are available, the MPC method can reduce the influences of the spatial heterogeneity caused by both mixed land cover types and density variations in vegetation cover to retrieve the LAI with improved accuracy. Therefore, (6) can be applied to correct regional moderate-resolution LAI products in regional studies when high-resolution gap proportion information is available.

### C. Applicability of the MPC Method

*1) Applicability of the MPC Method to Global LAI Products:* There are two ways to apply the MPC method to global MODIS LAI products. One is to directly generate the global LAI products (i.e., $L_m$) based on the MODIS LAI retrieval algorithm and (8). The other is to correct the already produced MODIS LAI product using the MPCF. When the global LAI product is directly generated using the MPC method, the high-resolution land cover maps (e.g., FROM-GLC maps) can be projected to the sinusoidal projection of the MCD12Q1 product and provide information on the biome combination and proportion of each biome type within a MODIS pixel. Then, $L_{\text{model\_bio}\_i}$ in (8) can be calculated based on the MODIS operational algorithm. Finally, the MPC method can be used to produce the global LAI product using (8).

When the MODIS LAI product has already been generated, the MPCF can be calculated from one of the high-quality MODIS reflectance data within a small period (e.g., four or eight days) and the high-resolution land cover maps using (5). Then, the MPCF can be used to correct the MODIS LAI product using (6). The computing time to correct the existing MODIS LAI product is only 1/16 of the computing time (when the period is eight days) to reproduce the corresponding LAI product using the MPC method.

In addition, according to the theory of the MPC method, the MPC method can also be used to correct other moderate- and low-resolution LAI products once the land cover types are used as the input parameters in the operational algorithm of the corresponding LAI products.

The performance of the MODIS LAI algorithm at VAERI sites may be worse than previously reported (such as the study by Yan et al. [70]). This is likely because the validation data selected in this manuscript are more heterogeneous than those used in previous studies. In the selection of the validation site in this article, the validation results are only used when DVTP<0.9 to ensure pixel heterogeneity since the MPC method is proposed to improve the accuracy of LAI retrievals

for mixed pixels. In contrast, the sites with strong heterogeneity were screened out in the selection of validation sites in the study by Yan et al. [70]. The MODIS LAI algorithm performs worse in regions with strong heterogeneity than in homogeneous regions, as reported in previous studies [41], [44], [45], [46], [47].

Since the modified Beer's law used in the derivation of the MPC method assumes leaves with 100% absorption, which is almost valid in the visible domain but not in the near-infrared domain, the MPC method should meet the requirements of the modified Beer's law when it is applied to produce global LAI products. Since the gap proportion information in (6) can be calculated in the visible band based on the 3DRT model, and LAI is a band-independent vegetation structure parameter that can be measured by optical instruments (e.g., TRAC) using canopy gap information [71], the derived equations of the MPC method [i.e., (6) and (8)] can meet the requirements of modified Beer's law when the MPC method is applied to produce MODIS LAI products. The proposed MPC method may not be applicable when the gap proportion information of the visible band cannot be calculated by the LAI inversion model. In future studies, we will focus on investigating a semiphysical canopy model that is also feasible in the near-infrared domain to improve the applicable range of the MPC method.

*2) Applicability of the MPC Method in Terms of Spatial Heterogeneity and Computational Efficiency:* For a mixed pixel composed of $n_b$ biome types, the computing time of LAI retrievals using the MPC method is positively correlated with the number of biome types in the mixed pixel (approximately $n_b$ times the computing time of LAI retrievals using the MODIS operational algorithm). Thus, the computing time of LAI retrievals using the MPC method is approximately 2.78 times that of the MODIS operational algorithm.

As shown in Figs. 6 and 7, the MOD LAI retrievals were similar to the MPC LAI retrievals for the relatively homogenous pixels (DVTP $\geq$ 0.9). Those relatively homogenous pixels were also regarded as "pure" pixels in the study by Yin et al. [51]. Therefore, using the MODIS main algorithm instead of the MPC method to directly retrieve the LAI of those pixels (DVTP $\geq$ 0.9) may be an effective method to reduce the computing time in the generation of global LAI products. Thus, the computing time was reduced to 1.63 times that of the MODIS operational algorithm. If the MPC method is used to correct the existing four-day MODIS LAI products based on the MPCF, the computing time can be further reduced to 0.20 times that of the MODIS operational algorithm. The MPC method is also feasible in terms of computational efficiency compared with the operational algorithms of the current moderate-resolution LAI products.

## VI. CONCLUSION

Spatial heterogeneity in moderate-resolution pixels leads to large errors in the retrieval of moderate-resolution LAI products. In this study, the MPC method was proposed to reduce the influences of spatial heterogeneity to improve the accuracy of LAI retrievals over heterogeneous areas with a

mixture of different biome types. The DART-simulated LAI, the aggregated Landsat LAI, and site-based high-resolution LAI reference maps were used to evaluate the performance of the proposed MPC method. The results indicate the following.

1) The MOD LAI was overestimated for forest-dominated pixels mixed with a large proportion of herbaceous vegetation and underestimated for herbaceous vegetation-dominated pixels mixed with a large proportion of forest. The MPC method can reduce the effect of mixed land cover types to improve the accuracy of LAI retrievals, especially for forest-grass transition zones.

2) The MOD LAI retrievals deviated from the reference LAI values when incorrect land cover types were used as the input biome types. The MPC method can reduce the influence of biome misclassification to obtain a more accurate LAI, given that the high-resolution land cover map is accurate.

3) The heterogeneity caused by the density variation in vegetation cover resulted in the underestimation of MOD LAI retrievals. The magnitude of underestimation increased with increasing heterogeneity. The MPC method can correct such underestimation when the gap proportion information of the high-resolution subpixels is available in the retrieval of moderate-resolution LAI products.

4) The RMSE (bias) decreased from 0.749 (0.486) to 0.414 (0.087), while the R2 increased from 0.084 to 0.524, and the proportion of pixels that fulfill the uncertainty requirement of the GCOS [<max(0.5, 20%)] increased from 38.2% to 84.6% for the results of site-based high-resolution LAI reference maps. The MPC method shows potential for improving the accuracy of global moderate-resolution LAI products over heterogeneous areas.

In this article, the MPC method was applied to correct the LAI estimated by the MODIS main algorithm as an example to explore the possibility of its application to the current global LAI product. However, it is still difficult to reduce the heterogeneity caused by the density variation in vegetation cover at the global scale due to the lack of global high-resolution gap proportion information. In future work, we will focus on producing global high-resolution FVC products to fill the data gap for the global high-resolution gap proportion information to further improve the accuracy of moderate-resolution LAI products over heterogeneous areas.

## REFERENCES

[1] J. M. Chen and T. A. Black, "Defining leaf area index for non-flat leaves," *Plant Cell Environ.*, vol. 15, no. 4, pp. 421–429, May 1992.

[2] J. Zhao, J. Li, Q. Liu, L. Yang, and J. Bai, "A method of analyzing LAI underestimation for dense vegetation based on the vertical distribution of the leaf area density," *Remote Sens. Lett.*, vol. 9, no. 2, pp. 121–130, Feb. 2018.

[3] G. Yan et al., "Review of indirect optical measurements of leaf area index: Recent advances, challenges, and perspectives," *Agricult. Forest Meteorol.*, vol. 265, pp. 390–411, Feb. 2019.

[4] *Systematic Observation Requirements for Satellite-Based Products for Climate, 2011 Update, Supplemental Details to the Satellite-Based Component of the Implementation Plan for the Global Observing System for Climate in Support of the UNFCCC (2010 Update)*, GCOS, World Meteorological Org., Geneva, Switzerland, 2011.

[5] A. K. Skidmore et al., "Environmental science: Agree on biodiversity metrics to track from space," *Nature*, vol. 523, pp. 403–405, Jul. 2015.

[6] M. Claverie, J. Matthews, E. Vermote, and C. Justice, "A 30+ year AVHRR LAI and FAPAR climate data record: Algorithm description and validation," *Remote Sens.*, vol. 8, no. 3, p. 263, Mar. 2016.

[7] J. Zhao et al., "Estimating fractional vegetation cover from leaf area index and clumping index based on the gap probability theory," *Int. J. Appl. Earth Observ. Geoinf.*, vol. 90, Aug. 2020, Art. no. 102112.

[8] D. B. Clark, P. C. Olivas, S. F. Oberbauer, D. A. Clark, and M. G. Ryan, "First direct landscape-scale measurement of tropical rain forest leaf area index, a key driver of global primary productivity," *Ecology Lett.*, vol. 11, pp. 163–172, Feb. 2008.

[9] H. Jin, A. Li, J. Wang, and Y. Bo, "Improvement of spatially and temporally continuous crop leaf area index by integration of CERES-maize model and MODIS data," *Eur. J. Agron.*, vol. 78, pp. 1–12, Aug. 2016.

[10] J. M. Sabater, C. Rüdiger, J.-C. Calvet, N. Fritz, L. Jarlan, and Y. Kerr, "Joint assimilation of surface soil moisture and LAI observations into a land surface model," *Agricult. Forest Meteorol.*, vol. 148, nos. 8–9, pp. 1362–1373, 2008.

[11] V. Arora, "Modeling vegetation as a dynamic component in soil-vegetation-atmosphere transfer schemes and hydrological models," *Rev. Geophys.*, vol. 40, no. 2, pp. 3-1–3-26, May 2002.

[12] G. P. Asner, J. M. O. Scurlock, and J. A. Hicke, "Global synthesis of leaf area index observations: Implications for ecological and remote sensing studies," *Global Ecol. Biogeogr.*, vol. 12, pp. 191–205, May 2003.

[13] R. E. Dickinson, "Land processes in climate models," *Remote Sens. Environ.*, vol. 51, no. 1, pp. 27–38, Jan. 1995.

[14] P. J. Sellers et al., "Modeling the exchanges of energy, water, and carbon between continents and the atmosphere," *Science*, vol. 275, pp. 502–509, Jan. 1997.

[15] Y. Tian et al., "Exploring scale-dependent ecohydrological responses in a large endorheic river basin through integrated surface water-groundwater modeling," *Water Resour. Res.*, vol. 51, pp. 4065–4085, Jun. 2015.

[16] R. B. Myneni et al., "Global products of vegetation leaf area and fraction absorbed PAR from year one of MODIS data," *Remote Sens. Environ.*, vol. 83, pp. 214–231, Nov. 2002.

[17] D. Huang et al., "Stochastic transport theory for investigating the three-dimensional canopy structure from space measurements," *Remote Sens. Environ.*, vol. 112, pp. 35–50, Jan. 2008.

[18] Z. Xiao, S. Liang, J. Wang, Y. Xiang, X. Zhao, and J. Song, "Long-time-series global land surface satellite leaf area index product derived from MODIS and AVHRR surface reflectance," *IEEE Trans. Geosci. Remote Sens.*, vol. 54, no. 9, pp. 5301–5318, Sep. 2016.

[19] F. J. García-Haro et al., "Derivation of global vegetation biophysical parameters from EUMETSAT polar system," *ISPRS J. Photogramm. Remote Sens.*, vol. 139, pp. 57–74, May 2018.

[20] K. Yan et al., "Generating global products of LAI and FPAR from SNPP-VIIRS data: Theoretical background and implementation," *IEEE Trans. Geosci. Remote Sens.*, vol. 56, pp. 2119–2137, Jan. 2018.

[21] F. Baret et al., "LAI, fAPAR and fCover CYCLOPES global products derived from VEGETATION—Part 1: Principles of the algorithm," *Remote Sens. Environ.*, vol. 110, pp. 275–286, Oct. 2007.

[22] F. Baret et al., "GEOV1: LAI and FAPAR essential climate variables and FCOVER global time series capitalizing over existing products. Part1: Principles of development and production," *Remote Sens. Environ.*, vol. 137, pp. 299–309, Oct. 2013.

[23] L. A. Brown et al., "Evaluation of global leaf area index and fraction of absorbed photosynthetically active radiation products over North America using Copernicus ground based observations for validation data," *Remote Sens. Environ.*, vol. 247, Sep. 2020, Art. no. 111935.

[24] R. Lacaze et al., "Operational 333 m biophysical products of the Copernicus global land service for agriculture monitoring," *Int. Arch. Photogramm., Remote Sens. Spatial Inf. Sci.*, vol. 47, no. W3, pp. 53–56, 2015.

[25] M. Tum et al., "Global gap-free MERIS LAI time series (2002–2012)," *Remote Sens.*, vol. 8, p. 69, Jan. 2016.

[26] H.-S. Kang, Y. Xue, and G. J. Collatz, "Impact assessment of satellite-derived leaf area index datasets using a general circulation model," *J. Climate*, vol. 20, no. 6, pp. 993–1015, Mar. 2007.

[27] S. Garrigues et al., "Validation and intercomparison of global leaf area index products derived from remote sensing data," *J. Geophys. Res., Biogeosci.*, vol. 113, pp. 1–20, Jun. 2008.

[28] H. Fang, S. Wei, and S. Liang, "Validation of MODIS and CYCLOPES LAI products using global field measurement data," *Remote Sens. Environ.*, vol. 119, pp. 43–54, Apr. 2012.

[29] F. Camacho, J. Cernicharo, R. Lacaze, F. Baret, and M. Weiss, "GEOV1: LAI, FAPAR essential climate variables and FCOVER global time series capitalizing over existing products. Part 2: Validation and inter-comparison with reference products," *Remote Sens. Environ.*, vol. 137, pp. 310–329, Oct. 2013.

[30] M. Claverie, E. F. Vermote, M. Weiss, F. Baret, O. Hagolle, and V. Demarez, "Validation of coarse spatial resolution LAI and FAPAR time series over cropland in southwest France," *Remote Sens. Environ.*, vol. 139, pp. 216–230, Dec. 2013.

[31] L. Guo, J. Wang, Z. Xiao, H. Zhou, and J. Song, "Data-based mechanistic modelling and validation for leaf area index estimation using multi-angular remote-sensing observation time series," *Int. J. Remote Sens.*, vol. 35, no. 13, pp. 4655–4672, Jul. 2014.

[32] H. Jin et al., "Intercomparison and validation of MODIS and GLASS leaf area index (LAI) products over mountain areas: A case study in southwestern China," *Int. J. Appl. Earth Observ. Geoinf.*, vol. 55, pp. 52–67, Mar. 2017.

[33] B. D. Xu et al., "Analysis of global LAI/FPAR products from VIIRS and MODIS sensors for spatio-temporal consistency and uncertainty from 2012–2016," *Forests*, vol. 9, p. 73, Feb. 2018.

[34] M. Weiss, F. Baret, S. Garrigues, and R. Lacaze, "LAI and fAPAR CYCLOPES global products derived from VEGETATION. Part 2: Validation and comparison with MODIS collection 4 products," *Remote Sens. Environ.*, vol. 110, no. 3, pp. 317–331, 2007.

[35] Z. Xiao, S. Liang, and B. Jiang, "Evaluation of four long time-series global leaf area index products," *Agricul. Forest Meteorol.*, vol. 246, pp. 218–230, Nov. 2017.

[36] C. Bacour, F. Baret, D. Béal, M. Weiss, and K. Pavageau, "Neural network estimation of LAI, fAPAR, fCover and LAI×cab, from top of canopy MERIS reflectance data: Principles and validation," *Remote Sens. Environ.*, vol. 105, no. 4, pp. 313–325, Dec. 2006.

[37] J. T. Morisette et al., "Validation of global moderate-resolution LAI products: A framework proposed within the CEOS land product validation subgroup," *IEEE Trans. Geosci. Remote Sens.*, vol. 44, no. 7, pp. 1804–1817, Jun. 2006.

[38] A. Verger, F. Baret, and M. Weiss, "Performances of neural networks for deriving LAI estimates from existing CYCLOPES and MODIS products," *Remote Sens. Environ.*, vol. 112, no. 6, pp. 2789–2803, Jun. 2008.

[39] X. Tao, S. Liang, and D. Wang, "Assessment of five global satellite products of fraction of absorbed photosynthetically active radiation: Intercomparison and direct validation against ground-based data," *Remote Sens. Environ.*, vol. 163, pp. 270–285, Jun. 2015.

[40] H. Fang, F. Baret, S. Plummer, and G. Schaepman-Strub, "An overview of global leaf area index (LAI): Methods, products, validation, and applications," *Rev. Geophys.*, vol. 57, no. 3, pp. 739–799, Sep. 2019.

[41] B. Xu et al., "Improving leaf area index retrieval over heterogeneous surface mixed with water," *Remote Sens. Environ.*, vol. 240, Apr. 2020, Art. no. 111700.

[42] W. Yang et al., "MODIS leaf area index products: From validation to algorithm improvement," *IEEE Trans. Geosci. Remote Sens.*, vol. 44, no. 7, pp. 1885–1898, Jun. 2006.

[43] H. Wu, B.-H. Tang, and Z.-L. Li, "Impact of nonlinearity and discontinuity on the spatial scaling effects of the leaf area index retrieved from remotely sensed data," *Int. J. Remote Sens.*, vol. 34, nos. 9–10, pp. 3503–3519, May 2013.

[44] Y. Tian, Y. Wang, Y. Zhang, Y. Knyazikhin, J. Bogaert, and R. B. Myneni, "Radiative transfer based scaling of LAI retrievals from reflectance data of different resolutions," *Remote Sens. Environ.*, vol. 84, no. 1, pp. 143–159, Jan. 2003.

[45] S. Garrigues, D. Allard, F. Baret, and M. Weiss, "Influence of landscape spatial heterogeneity on the non-linear estimation of leaf area index from moderate spatial resolution remote sensing data," *Remote Sens. Environ.*, vol. 105, no. 4, pp. 286–298, Dec. 2006.

[46] Z. Jin, Q. Tian, J. M. Chen, and M. Chen, "Spatial scaling between leaf area index maps of different resolutions," *J. Environ. Manage.*, vol. 85, no. 3, pp. 628–637, Nov. 2007.

[47] H. L. Fang, W. J. Li, and R. B. Myneni, "The impact of potential land cover misclassification on MODIS leaf area index (LAI) estimation: A statistical perspective," *Remote Sens.*, vol. 5, no. 2, pp. 830–844, Feb. 2013.

[48] J. M. Chen, "Spatial scaling of a remotely sensed surface parameter by contexture," *Remote Sens. Environ.*, vol. 69, no. 1, pp. 30–42, Jul. 1999.

[49] C. Jun, Y. Ban, and S. Li, "Open access to earth land-cover map," *Nature*, vol. 514, no. 7523, p. 434, 2014.

[50] W. Yu et al., "Global land cover heterogeneity characteristics at moderate resolution for mixed pixel modeling and inversion," *Remote Sens.*, vol. 10, p. 856, Jun. 2018.

[51] G. Yin et al., "Improving leaf area index retrieval over heterogeneous surface by integrating textural and contextual information: A case study in the Heihe River Basin," *IEEE Geosci. Remote Sens. Lett.*, vol. 12, no. 2, pp. 359–363, Aug. 2015.

[52] Y. Zeng et al., "A radiative transfer model for patchy landscapes based on stochastic radiative transfer theory," *IEEE Trans. Geosci. Remote Sens.*, vol. 58, no. 4, pp. 2571–2589, Apr. 2020.

[53] T. Nilson, "A theoretical analysis of the frequency of gaps in plant stands," *Agricult. Meteorol.*, vol. 8, pp. 25–38, Jan. 1971.

[54] S. Tang et al., "LAI inversion algorithm based on directional reflectance kernels," *J. Environ. Manage.*, vol. 85, pp. 638–648, Nov. 2007.

[55] J. P. Gastellu-Etchegorry, E. Martin, and F. Gascon, "DART: A 3D model for simulating satellite images and studying surface radiation budget," *Int. J. Remote Sens.*, vol. 25, no. 1, pp. 73–96, 2004.

[56] J. Gastellu-Etchegorry et al., "DART: Recent advances in remote sensing data modeling with atmosphere, polarization, and chlorophyll fluorescence," *IEEE J. Sel. Topics Appl. Earth Observ. Remote Sens.*, vol. 10, no. 6, pp. 2640–2649, Apr. 2017.

[57] F. Gascon, J.-P. Gastellu-Etchegorry, M.-J. Lefevre-Fonollosa, and E. Dufrene, "Retrieval of forest biophysical variables by inverting a 3-D radiative transfer model and using high and very high resolution imagery," *Int. J. Remote Sens.*, vol. 25, no. 24, pp. 5601–5616, Dec. 2004.

[58] A. Banskota et al., "Investigating the utility of wavelet transforms for inverting a 3-D radiative transfer model using hyperspectral data to retrieve forest LAI," *Remote Sens.*, vol. 5, pp. 2639–2659, May 2013.

[59] Z. Malenovsky et al., "Influence of woody elements of a Norway spruce canopy on nadir reflectance simulated by the DART model at very high spatial resolution," *Remote Sens. Environ.*, vol. 112, pp. 1–18, Jan. 2008.

[60] J. P. Gastellu-Etchegorry et al., "Modeling BRF and radiation regime of boreal and tropical forests: I. BRF," *Remote Sens. Environ.*, vol. 68, pp. 281–316, Jun. 1999.

[61] J. Widlowski et al., "The fourth phase of the radiative transfer model intercomparison (RAMI) exercise: Actual canopy scenarios and conformity testing," *Remote Sens. Environ.*, vol. 169, pp. 418–437, Nov. 2015.

[62] S. Duthoit, V. Demarez, J.-P. Gastellu-Etchegorry, E. Martin, and J.-L. Roujean, "Assessing the effects of the clumping phenomenon on BRDF of a maize crop based on 3D numerical scenes using DART model," *Agricult. Forest Meteorol.*, vol. 148, pp. 1341–1352, Jul. 2008.

[63] C. Li et al., "The first all-season sample set for mapping global land cover with Landsat-8 data," *Sci. Bull.*, vol. 62, pp. 508–515, Apr. 2017.

[64] P. Gong et al., "Stable classification with limited sample: Transferring a 30-m resolution sample set collected in 2015 to mapping 10-m resolution global land cover in 2017," *Sci. Bull.*, vol. 64, pp. 370–373, Jan. 2019.

[65] P. Gong et al., "Finer resolution observation and monitoring of global land cover: First mapping results with Landsat TM and ETM+ data," *Int. J. Remote Sens.*, vol. 34, pp. 2607–2654, Apr. 2012.

[66] M. A. Friedl et al., "MODIS Collection 5 global land cover: Algorithm refinements and characterization of new datasets," *Remote Sens. Environ.*, vol. 114, pp. 168–182, Jan. 2010.

[67] J. G. Masek et al., "A Landsat surface reflectance dataset for North America, 1990–2000," *IEEE Geosci. Remote Sens. Lett.*, vol. 3, no. 1, pp. 68–72, Jan. 2006.

[68] B. Xu et al., "Evaluating spatial representativeness of station observations for remotely sensed leaf area index products," *IEEE J. Sel. Topics Appl. Earth Observ. Remote Sens.*, vol. 9, no. 7, pp. 3267–3282, Jun. 2016.

[69] B. Chen et al., "Characterizing spatial representativeness of flux tower eddy-covariance measurements across the Canadian carbon program network using remote sensing and footprint analysis," *Remote Sens. Environ.*, vol. 124, pp. 742–755, Sep. 2012.

[70] K. Yan et al., "Evaluation of MODIS LAI/FPAR product collection 6. Part 2: Validation and intercomparison," *Remote Sens.*, vol. 8, p. 460, May 2016.

[71] J. M. Chen and J. Cihlar, "Plant canopy gap-size analysis theory for improving optical measurements of leaf-area index," *Appl. Opt.*, vol. 34, no. 27, pp. 6211–6222, 1995.
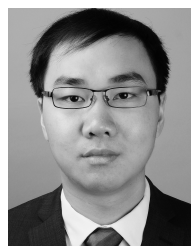
**Yadong Dong** received the B.S., M.S., and Ph.D. degrees in cartography and geography information systems from the Faculty of Geographical Science, Beijing Normal University, Beijing, China, in 2011, 2014, and 2017, respectively.

He was a Post-Doctoral Fellow with the College of Water Sciences, Beijing Normal University, from 2017 to 2019. He is currently an Assistant Researcher with the State Key Laboratory of Remote Sensing Science, Aerospace Information Research Institute, Chinese Academy of Sciences, Beijing. His research focus is on optical radiative transfer modeling and vegetation parameter inversion methods.

**Jing Li** received the B.S. degree in geology from Zhejiang University, Hangzhou, China, in 2002, and the Ph.D. degree in cartography and geographic information systems from the Graduate University of the Chinese Academy of Sciences, Beijing, China, in 2007.

She was a Visiting Scholar with Wageningen University & Research, Wageningen, The Netherlands, from 2008 to 2009, and the Plant Functional Biography and Climate Change Cluster, University of Technology Sydney, Sydney, NSW, Australia, in 2014. She is currently an Associate Professor with the State Key Laboratory of Remote Sensing Science, Aerospace Information Research Institute, Chinese Academy of Sciences, Beijing. She is also with the College of Resources and Environment, University of Chinese Academy of Sciences, Beijing. Her primary research interests include optical radiative transfer modeling, vegetation parameter inversion methods from remote sensing, agricultural applications of remote sensing, and vegetation change detection.

**Ziti Jiao** received the B.Sc. degree in mining engineering from the Wuhan Institute of Technology, Wuhan, Hubei, China, in 1993, the M.Sc. degree from the School of Geography, Beijing Normal University (BNU), Beijing, China, in 2002, the Ph.D. degree in geographic information systems from BNU in 2008, and the Ph.D. degree in remote sensing from Boston University (BU), Boston, MA, USA, in 2009.

He is currently a Professor with the Faculty of Geographical Science, Institute of Remote Sensing Science and Engineering, BNU. His research interests mainly include modeling reflectance anisotropy and albedo using remotely sensed data to monitor the reflectance characteristics of various land surfaces. More recently, he has been focused on the development of kernel-driven bidirectional reflectance distribution function (BRDF) models, including modeling the hotspot effect and snow scattering optics in the kernel-driven BRDF model framework. He is now working on the development of operational clumping index (CI) products to monitor the Earth's environment using multiangle signatures.

**Qinhuo Liu** (Senior Member, IEEE) received the B.Sc. degree in hydrogeology and engineering geology from Southwest Jiaotong University, Chengdu, China, in 1988, and the M.Sc. degree in cartography and remote sensing and the Ph.D. degree in atmospheric physics from Peking University, Beijing, China, in 1994 and 1997, respectively.

He was with the Institute of Remote Sensing Applications, Chinese Academy of Sciences, Beijing, from 1997 to 2012. He was a Visiting Scholar with Institut Nationale de la Recherche Agronomigue (INRA), Paris, France, in 1998; Boston University, Boston, MA, USA, in 1999; the University of Maryland, College Park, MD, USA, in 2004; George Mason University, Fairfax, VA, USA, in 2010; and the University of Technology Sydney, Sydney, NSW, Australia, in 2014. He is currently a Professor and the Executive Deputy Director of the State Key Laboratory of Remote Sensing Science, Aerospace Information Research Institute, Chinese Academy of Sciences, Beijing. He is also with the College of Resources and Environment, University of Chinese Academy of Sciences, Beijing. He has been a Principal Investigator for several major projects, including the National Key Research and Development Project, the Natural Science Foundation Key Project, the National High Technology Research and Development Program, and the National Basic Research Program of China. His research interests focus on radiation transfer modeling and inversion, Earth surface radiation budgets, and energy balances.

Dr. Liu is also a Senior Member of the IEEE Geoscience and Remote Sensing Society (IEEE GRSS).

**Jing Zhao** received the M.S. degree in cartography and geographic information systems from Jilin University, Jilin, China, in 2009, and the Ph.D. degree in cartography and geographic information systems from the Institute of Remote Sensing and Digital Earth, Chinese Academy of Sciences, Beijing, China, in 2013.

She is currently an Associate Professor with the State Key Laboratory of Remote Sensing Science, Aerospace Information Research Institute, Chinese Academy of Sciences. Her main research interests include canopy saturation analysis and vegetation parameter inversion from remote sensing data.

**Baodong Xu** received the Ph.D. degree from the Institute of Remote Sensing and Digital Earth, Chinese Academy of Sciences, Beijing, China, in 2018.

Since 2018, he has been an Associate Professor with the Macro Agriculture Research Institute, College of Resource and Environment, Huazhong Agricultural University, Wuhan, China. His research interests include biophysical variable estimation, validation of remote sensing products, and remote sensing applications in agriculture.

**Hu Zhang** received the B.S. degree from Shandong Jianzhu University, Shandong, China, in 2009, and the M.S. and Ph.D. degrees in geography from Beijing Normal University, Beijing, China, in 2012 and 2015, respectively.

He is currently an Associate Professor with the School of Geographic and Environmental Sciences, Tianjin Normal University, Tianjin, China. His research interests include land surface reflectance anisotropy classification and land surface albedo retrieval based on prior knowledge.

**Zhaoxing Zhang** received the B.E. and M.E. degrees in agricultural resources and environment from Shihezi University, Xinjiang, China, in 2016 and 2018, respectively.

He is currently a Research Intern with the State Key Laboratory of Remote Sensing Science, Aerospace Information Research Institute, Chinese Academy of Sciences, Beijing, China. His main research interests are agricultural remote sensing and the coupled application of crop growth models and remote sensing data.

**Chang Liu** received the B.S. degree in geomatics engineering from Nanjing Normal University, Nanjing, China, in 2019. She is currently pursuing the Ph.D. degree in cartography and geographic information systems with the Aerospace Information Research Institute, Chinese Academy of Sciences, Beijing, China, and also with the College of Resources and Environment, University of Chinese Academy of Sciences, Beijing.

Her research interests include leaf area index product validation and global climate change.

**Yuri Knyazikhin** received the M.S. degree in applied mathematics from the University of Tartu, Tartu, Estonia, in 1978, and the Ph.D. degree in numerical analysis from the N. I. Muskhelishvili Institute of Computing Mathematics, Georgian National Academy of Sciences, Tbilisi, Georgia, in 1985.

He was a Research Scientist with the Institute of Astrophysics and Atmospheric Physics, University of Tartu, and the Computer Center of the Siberian Branch, Russian Academy of Sciences, Moscow, Russia, from 1978 to 1990. He was an Alexander von Humboldt Fellow from 1990 to 1996. He is currently a Research Professor with the Department of Geography, Boston University, Boston, MA, USA. His work was published in the areas of numerical integral and differential equations, theory of radiative transfer in atmospheres and plant canopies, remote sensing of the atmosphere and plant canopies, ground-based radiation measurements, forest ecosystem dynamics, and modeling multifunctional forest management.

**Ranga B. Myneni** received the Ph.D. degree in biology from the University of Antwerp, Antwerp, Belgium, in 1985.

He is currently a Professor with Boston University, Boston, MA, USA. He is a Science Team Member of NASA Moderate Resolution Imaging Spectroradiometer (MODIS) and Visible Infrared Imaging Radiometer Suite (VIIRS) projects. He has authored or coauthored over 250 scientific articles in peer-reviewed journals. His research interests include remote sensing of vegetation and climate–vegetation interactions.